Geologische Bundesanstalt

Chair In Petroleum Geology

Determination of the origin of hydrocarbons in Austria using compound-specific isotope analysis

Projekttitel	**Herkunftsbestimmung von Kohlenwasserstoffen in Österreich mittels komponentenspezifischer Isotopie**
Projektleitung	Univ.-Prof. Dr.mont. Reinhard **Sachsenhofer**[1)]
Projektmitarbeiter	Prov.Doz. Dr. Achim **Bechtel**[1)] Dr. Reinhard **Gratzer** [1)] Mag. Piotr **Lipiarski**[2)]
Zeitraum	Januar 2018- Dezember 2018
Finanzierung	Im Rahmen der Initiative GBA-Forschungspartnerschaften Mineralrohstoffe

1) Montanuniversität Leoben, Lehrstuhl für Erdölgeologie
2) Geologische Bundesanstalt; Fachabteilung Rohstoffgeologie

Zusammenfassung

Öl-Muttergesteins-Korrelationen basieren meist auf Biomarker Daten und Isotopenverhältnissen der gesättigten und aromatischen Kohlenwasserstofffraktionen. Isotopenmuster, die auf der Kohlenstoffisotopie einzelner *n*-Alkane und Isoprenoids beruhen („compound specific isotopy"; CSI), stellen ein weiteres, aber selten benutztes Werkzeug für die Öl-Muttergesteins-Korrelation dar.

Im Rahmen der Studie wurden CSI Muster von 62 Gesteins- und 65 Ölproben aus unterschiedlichen geologischen Einheiten Österreichs (und Deutschlands) zusammengestellt. Die meisten Gesteinsproben sind oligozänen Alters, aber mesozoische und eozäne Gesteine wurden ebenfalls untersucht.

Die Studienergebnisse zeigen, dass die untersuchten Gesteine sehr unterschiedliche CSI Muster aufweisen. Detaillierte Untersuchungen des Unteroligozäns im Molasse Becken zeigen, dass die Isotopenverhältnisse von kurz-, mittel- und langkettigen *n*-Alkanen mit der stratigraphischen Position stark schwanken. Sehr negative Isotopenverhältnisse mittelkettiger *n*-Alkane führen zu einer spezifischen V-Form, die für Gesteine charakteristisch sind, die während der Nannoplankton-Zonen NP21, NP22 und der frühen NP23 abgelagert wurden. Eozäne Gesteine und jüngere oligozäne Einheiten weisen das V-Muster nicht auf. Die Faktoren, die die unterschiedlichen Isotopenmuster steuern werden bisher nicht wirklich verstanden.

CSI Muster der Ölproben weisen eine ähnlich hohe Variabilität auf. Sie belegen, dass die Schöneck-Formation das wichtigste Muttergestein der Molasseöle ist. Erstaunlicherweise beeinflusst die Eggerding-Formation die CSI Muster nicht. Während alle ökonomisch relevanten Öle durch die Schöneck-Formation generiert wurden, besitzen Ölspuren östlich der Enns in der Flysch Zone (Kleinraming), dem Molasse Becken (Mank) und in den Nördlichen Kalkalpen (Urmannsau) ein anderes, vermutlich mesozoisches Muttergestein.

Die neuen CSI Daten bilden eine wertvolle Basis für künftige Öl-Muttergesteins-Korrelationen. Trotzdem wurden wichtige stratigraphische Horizonte noch nicht untersucht. Wir schlagen daher folgende Nachfolge-Untersuchungen vor:

- Untersuchung weiterer Einheiten mit hohem Anteil organischen Materials:
    - "Seefelder Schichten" (Trias, Kalkalpen)
    - „Kössener Mergel" (Trias, Kalkalpen)
    - „Bitumenmergel" (Kreide, Kainacher Gosau)
    - "Bitumenmergel" (Oligozän, Inntal-Tertiär)

- Öle des Wiener Beckens wurden vor allem durch die oberjurassische Mikulov-Formation generiert. Allerdings wurde auch ein Beitrag oligozäner Gesteine diskutiert. Oberjura und Oligozän weisen deutlich unterscheidbare CSI Muster auf. Es ist daher zu erwarten, dass CSI Muster Aussagen hinsichtlich der relativen Anteile der beiden potentiellen Muttergesteine erlauben.
- Öle in Bohrungen östlich der Enns (Kleinraming, Mank, Urmannsau) weisen vermutlich ein mesozoisches Muttergestein auf. Wir schlagen daher systematische Untersuchungen des Muttergesteinspotentials der gesamten kalkalpinen Schichtfolge vor.
- CSI Muster der unteroligozänen Schichtfolge im Molasse Becken zeigen klare stratigraphische Trends. Trotz der durchgeführten hochauflösenden Untersuchungen, sind die Prozesse, die zur Veränderung der Isotopenverhältnisse führen, noch nicht verstanden. Es besteht daher ein dringender diesbezüglicher Forschungsbedarf.

Abstract

Oil-source correlations are often based on biomarker data and isotope ratios of saturated and aromatic hydrocarbon fractions. Isotope patterns based on carbon isotope ratios determined on specific n-alkanes and isoprenoids (compound-specific isotope analysis; CSIA) provide an additional, but rarely used tool for oil-source correlations.

In the frame of the present study, CSI patterns of 62 rock and 65 oil samples from different geological units in Austria (and Germany) area have been compiled. Most rock samples are Oligocene in age, but Mesozoic and Eocene rocks are also considered.

The study results show that rock samples display a wide range of CSI patterns and that these patterns differ significantly depending on the stratigraphy position of the investigated unit.

Detailed investigations of Lower Oligocene units in the Molasse Basin show that isotope ratios of short-, medium-, and long-chain n-alkanes differ significantly through time. Because of very negative isotope ratios of medium-chain n-alkanes, CSI patterns of rocks deposited during nanoplankton zones NP21, NP22 and the lower part of NP23 are characterized by specific V-shaped CSI patterns. These patterns are not observed in Eocene and overlying Oligocene rocks (upper part of NP23, NP24). The factors responsible for the different pattern and their changes are not fully understood yet.

CSI patterns of oil samples show similar high variations. They show that the Schöneck Formation is the main source rock in the Molasse Basin. Interestingly the Eggerding Formation has no influence on observed CSI patterns. Whereas all economic oil accumulations have been charged by the Schöneck Formation, oil and oil stains east of the river Enns in the Flysch Zone (Kleinraming), Molasse Basin (Mank) and the Northern Calcareous Alps (Urmannsau) have a different, probably Mesozoic source.

The presented data form a valuable base for future oil-source correlations. However, important stratigraphic have not been examined yet. Hence, we propose the following future investigations:

- Investigation of additional organic matter-rich units:
    - Triassic "Seefeld Beds" (Northern Calcareous Alp; NCA)
    - Triassic Kössen Marl (NCA)
    - Cretaceous bituminous marls (Kainach Gosau)
    - Early Oligocene "bituminous marls" in the Inntal Valley
- Vienna Basin oils have been generated mainly by the Upper Jurassic Mikulov Formation, but a contribution from Oligocene rocks has been postulated. These units yield largely different CSI patterns. Therefore, it can be expected that CSI data will allow the quantification of the relative contributions of both potential source units.
- Oils at Mank, Urmannsau and Kleinraming(?) probably have a Mesozoic source. We suggest a systematic investigation of the entire stratigraphy of the Northern Calcareous Alps to test their hydrocarbon potential.
- More investigations are needed to determine the source of oil in the Autochthonous Mesozoic.
- CSI patterns of Lower Oligocene rocks in the Molasse Basin show a clear stratigraphic trend. Despite of detailed investigations, the processes which result in different CSI patterns are still poorly understood and need additional investigations.

Table of Contents

1. INTRODUCTION

Oil-source correlations are traditionally based on biomarker data and isotope ratios of oil fractions (saturated and aromatic hydrocarbons). Isotope patterns based on carbon isotope ratios determined on specific n-alkanes and isoprenoids (compound-specific isotope analysis; CSIA) provide an additional, but rarely used tool for oil-source correlations (e.g. Pedentchouk and Turich, 2017). Bechtel et al. (2017) showed that in the Molasse Basin CSI data of different hydrocarbon deposits differ significantly. Isotope patterns, therefore, have a great potential for improved oil-source correlations. Hence, aims of the project "Herkunftsbestimmung von Kohlenwasserstoffen in Österreich mittels komponentenspezifischer Isotopie", performed within the "Initiative GBA-Forschungspartnerschaften Mineralrohstoffe" are:

- Further development of a technique for oil-source correlations (compound-specific isotope analysis; CSIA). Particularly, it was planned to study the causes for different isotope patterns.
- Determination of CSI patterns of oil and rock extracts from potential source rocks samples.
- Application of CSIA to determine the origin of oil and oil traces in Austria.

It has been agreed that CSI patterns of 15 source rock and 15 oil samples will be in investigated within the frame of the project. Results of these samples are included in the present report together with results from 43 oil samples, which were investigated within the frame a pilot study (Bechtel et al., 2013). Moreover, 11 rocks samples from Bavaria are included in the study. Overall, CSI data from 62 rock samples and 65 oil samples are considered in the report. Many of them have been acquired within the frame of a master´s thesis (Sweda, 2018).

The original plan was to study a wide variety of organic matter-rich rocks in Austria. However, because it became clear that different Oligocene units show variable CSI patterns, we strongly focussed the efforts on Lower Oligocene rocks.

2. SAMPLES

26 (Upper Eocene and) Oligocene samples from the Upper Austrian part of the Molasse Basin have been investigated. For comparison, 7 additional rock samples with an Early Oligocene age from the German sector of the basin have been included in the study together with 3 Lower Oligocene rocks in the Waschberg Zone (borehole Thomasl; Lower Austria).

Mesozoic rocks are represented by Triassic Reifling Limestone (Falkenstein tunnel near Klaus) and Hauptdolomite (Witzala), Lower Jurassic Bächental Formation (Bächental) and Upper Jurassic Mikulov Formation (Zistersdorf, Maustrenk). For comparison, four Jurassic rock samples from the Jura Mountains in Germany have been invesitgated.

Oil samples (and borehole cores with oil stains) have been provided by RAG and OMV. Stored samples from abandoned fields have been provided by the Geological Survey of Austria (GBA).

Locations of rock and oil samples are shown in Fig. 1. Tables 1 and 2 provide information on location, depth, stratigraphy and some key parameters (TOC, HI, Tmax) of the studied rock samples. Table 3 summarizes information on oil samples. Additional information may be found in the references cited in the tables.

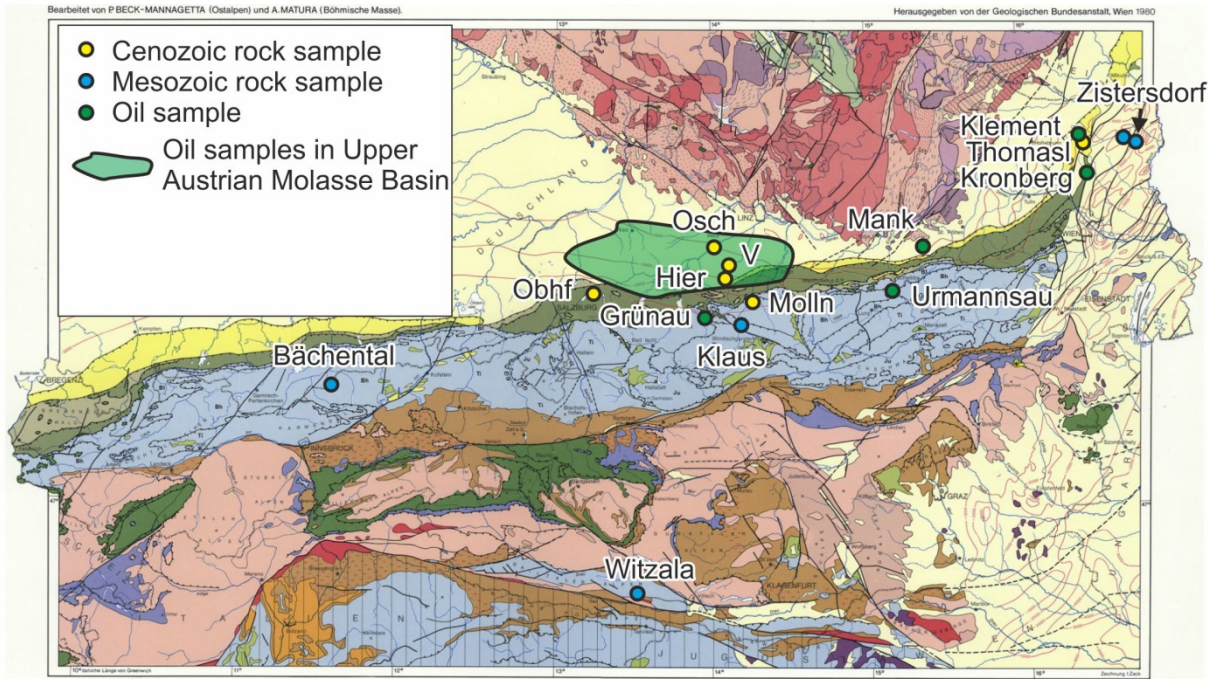

Fig. 1. Map with sample locations (backgrond geology: GBA). Location of rock samples from Germany are not shown.

Table 1: Overview of Cenozoic rock samples

Well / Location	Source	Sample type	Depth / Height (m)	Age	Stratigraphy	TOC	HI	Tmax
German Molasse Basin (Pupp, 2018)								
West Molasse								
Well A	Exxon	core	2133.57	Early Oligocene	Dynow Fm.	2.37	644	432
Well A	Exxon	core	2136.15	Early Oligocene	Schöneck “c”	8.58	637	436
Well A	Exxon	core	2137.45	Early Oligocene	Schöneck “c”	4.30	514	430
Well A	Exxon	core	2138.50	Early Oligocene	Schöneck “c”	2.15	473	428
East Molasse								
Well C	Exxon	core	2449.87	Early Oligocene	Schöneck “c”?	7.45	522	419
Well C	Exxon	core	2451.27	Early Oligocene	Schöneck “b”	3.23	443	415
Well C	Exxon	core	2452.5	Early Oligocene	Schöneck “b”	3.37	515	413
Austrian Molasse Basin (Schulz et al., 2002; Sachsenhofer et al., 2010; Bechtel et al., 2013)								
Hier-4	RAG	cuttings	2400	Early Oligocene	Zupfing Fm.	0,99	125	431
Hier-4	RAG	cuttings	2420	Early Oligocene	Eggerding Fm.	1,72	233	428
Hier-4	RAG	cuttings	2425	Early Oligocene	Eggerding Fm.	1,51	231	429
Hier-4	RAG	cuttings	2435	Early Oligocene	Eggerding Fm.	1,90	258	427
Osch-1	RAG	core	1369.17	Early Oligocene	Eggerding Fm.	5.99	578	421
Osch-1	RAG	core	1371.22	Early Oligocene	Eggerding Fm.	3.56	552	424
Osch-1	RAG	core	1373.29	Early Oligocene	Dynow Fm.	1,84	535	429
Osch-1	RAG	core	1375.82	Early Oligocene	Dynow Fm.	2,39	600	425
Osch-1	RAG	core	1377.28	Early Oligocene	Dynow Fm.	4,67	542	418
Osch-1	RAG	core	1379.9	Early Oligocene	Dynow Fm.	1,84	535	429
Osch-1	RAG	core	1381.79	Early Oligocene	Dynow/Schöneck Fm.	2,39	600	425
Osch-1	RAG	core	1382.05	Early Oligocene	Schöneck “c”	4,67	542	418
Osch-1	RAG	core	1382.49	Early Oligocene	Schöneck “c”	4,32	612	424
Osch-1	RAG	core	1383.96	Early Oligocene	Schöneck “c”	4,95	602	423
Osch-1	RAG	core	1384.46	Early Oligocene	Schöneck “c”	10,10	540	424
Osch-1	RAG	core	1385.45	Early Oligocene	Schöneck “c”	4,60		
Osch-1	RAG	core	1387.7	Early Oligocene	Schöneck “b”	2,42	505	406
Osch-1	RAG	core	1389.24	Early Oligocene	Schöneck “b”	2,95	501	411
Osch-1	RAG	core	1390.75	Early Oligocene	Schöneck “a”	1,77	385	421
Osch-1	RAG	core	1392.87	Early Oligocene	Schöneck “a”	2,00	399	417
BHN-2	RAG	core	1865.48	Late Eocene	Certithian Beds	1.74	322	438
BHN-2	RAG	core	1866.78	Late Eocene	Certithian Beds	5.95	557	434
Molln-1	OMV	cuttings	5190	Early Oligocene	Schöneck Fm.			
Molln-1	OMV	cuttings	5200	Early Oligocene	Schöneck Fm.			
Obhf-1 (545)	RAG	core	4293	Early Oligocene	Schöneck (Obhf facies)	1.58	306	440
Obhf-1 (540)	RAG	core	4295	Early Oligocene	Schöneck (Obhf facies)	1.80	371	443
Waschberg Zone (Austria; Pupp et al., 2018)								
Thomasl-1	OMV	cuttings	1650	Oligocene	Thomasl Fm., NP24	1.88	165	424
Thomasl-1	OMV	cuttings	1720	Oligocene	Thomasl Fm., NP24	2.66	223	418
Thomasl-1	OMV	cuttings	1760	Oligocene	Thomasl Fm., NP24	3.33	116	426

Table 2: Overview of Mesozoic rock samples

Well / Location	Source	Sample type	Depth / Height (m)	Age	Stratigraphy	TOC	HI	Tmax
German Jura Mountains (Drews, in prep.)								
Mistelgau (MG)		quarry		E.Jura. (Late Toarc.)	Jurensis Marl	1.29	100	428
Dotternhausen		quarry		E. Jura. (Toarcian)	Posidonia Shale			
Schönlind; SL-H		quarry		E. Jurassic (Pliensb.)	Amaltheen-Ton	1.58	170	429
Schönlind; SL-S		quarry		E. Jurassic (Pliensb.)	Amaltheen-Ton	1.38	129	427
Calcareous Alps (Austria; Neumeister et al., 2015; Gratzer et al., 2015)								
Bächental (BT-35)		quarry	19.0	E. Jurassic (Toarcian	Bächental bitum. marl	9.3	666	422
Bächental (BT-26)		quarry	14.2	E. Jurassic (Toarcian	Bächental bitum. marl	7.6	653	424
Bächental (BT-25)		quarry	13.4	E. Jurassic (Toarcian	Bächental bitum. marl	12.8	622	421
Falkenstein T. KB-4		core		Triassic	Reifling Limestone			
Falkenstein T. KB-5		core		Triassic	Reifling Limestone			
Falkenstein T. KB-7		core		Triassic	Reifling Limestone			
Gailtal Alps (Austria; Abram, 2001)								
Witzala APII 1		outcrop	0.10	Triassic (Norian)	Hauptdolomit Fm.	0.6	56	430
Witzala APII 4		outcrop	0.3	Triassic (Norian)	Hauptdolomit Fm.	21.8	339	425
Witzala APII 6		outcrop	0.5	Triassic (Norian)	Hauptdolomit Fm.	0.94	410	434
Witzala APII 10		outcrop	0.9	Triassic (Norian)	Hauptdolomit Fm.	1.02	559	438
Witzala APII 20		outcrop	14	Triassic (Norian)	Hauptdolomit Fm.	0.48	337	431
Witzala APII 26		outcrop	25	Triassic (Norian)	Hauptdolomit Fm.	2.65	438	434
Witzala APII 37		outcrop		Triassic (Norian)	Hauptdolomit Fm.	2.43	453	436
Witzala APII 44		outcrop	41	Triassic (Norian)	Hauptdolomit Fm.	0.61	598	436
Witzala APII 48		outcrop	47.2	Triassic (Norian)	Hauptdolomit Fm.	0.45	600	435
Witzala APII 49		outcrop	52	Triassic (Norian)	Hauptdolomit Fm.	0.51	618	435
Witzala APII 52		outcrop	64.5	Triassic (Norian)	Hauptdolomit Fm.	0.34	600	438
Witzala APII 53		outcrop	66	Triassic (Norian)	Hauptdolomit Fm.	0.39	538	434
Vienna Basin (Austria; Rupprecht, 2017)								
Zistersdorf-ÜT1	OMV	core	5605.5	Late Jurassic	Mikulov Marlstone	1.18	126	449
Zistersdorf-ÜT1	OMV	core	5740.7	Late Jurassic	Mikulov Marlstone	1.76	141	453
Maustrenk-ÜT1	OMV	core	6546.7	Late Jurassic	Mikulov Marlstone	1.58	34	455
Maustrenk-ÜT1	OMV	core	6548.8	Late Jurassic	Mikulov Marlstone	1.21	57	454

Table 3: Overview of oil samples

Sample	Top (m)	Base (m)	Stratigraphy	Sampling	Remarks
Molasse Basin					
Kohleck-2	2240	2265,5	Upper Eocene		RAG
Kemating-W2			Upper Eocene		RAG
Kemating-1			Upper Eocene		RAG
Maria Schmolln-1	2095.5	2103		1973	GBA
Steindlberg-1	1909	1913.5	Up. Eocene (Litho.L.)	1958	GBA
Steindlberg-2	1909.5	1915.5		1959	GBA
Ried-5			Upper Eocene		RAG
Trat 7			Cenomanian		RAG
Trat 8			Cenomanian		RAG
Trat 10			Cenomanian		RAG
Puchkirchen-1	2581	2583	Upper Eocene	?	GBA
Schwanenstadt-2	1986.8	1993	Up. Eocene (Litho.L.)	1963	GBA
Wegscheid-1	2676	2680.9	Up. Eocene (Litho.L.)	?	GBA
Lindach-1					
Mühlreith	3257		Oligocene		RAG
BH-2			Upper Eocene		RAG
BH-9					RAG
BH-N1			Upper Eocene		RAG
BH-7					RAG
Kematen-1			Upper Eocene		RAG
Engenfeld-1	1054,2	1066,2	Upper Eocene	1968	GBA
Engenfeld-6			Upper Eocene		RAG
Piberbach-7					
Pfarrkirchen-1					RAG
Mayersdorf-1			Jurassic		RAG
Eberstalzell-2a	2065	2080	Upper Eocene	1967	GBA
Eberstalzell-6			Upper Eocene		RAG
Eberstalzell-7			Upper Eocene		RAG
Oberaustall-1			Cenomanian		RAG
Oberaustall-1	1837	1841	Upper Eocene	1971	GBA
Oberaustall-2	1944	1956	Cenomanian	1971	GBA
Sattledt-2			Upper Eocene		RAG
Sattledt-10			Upper Eocene		RAG
Sattledt-23			Upper Eocene		RAG
Rappersdorf-2			Upper Eocene		RAG
Steinhaus-6			Upper Eocene		RAG
Steinhaus-N2			Upper Eocene		RAG
Wels N1					
Vo 13			Upper Eocene		RAG
Vo 19			Upper Eocene		RAG
Vo 23			Upper Eocene		RAG
Vo 41			Upper Eocene		RAG
V-01			Upper Eocene		RAG
V-02			Upper Eocene		RAG
V-08			Upper Eocene		RAG
V-11			Upper Eocene		RAG
V-13			Upper Eocene		RAG
V-15			Upper Eocene		RAG
V-19			Upper Eocene		RAG
V-21			Upper Eocene		RAG
V-23			Upper Eocene		RAG
V-33			Upper Eocene		RAG
V-39			Upper Eocene		RAG
V-41			Upper Eocene		RAG

Table 3: Overview of oil samples (continued)

Sample	Top (m)	Base (m)	Stratigraphy	Sampling	Remarks
Sierning-1					RAG
Wirnzberg-1					OMV
Gruenau-1	~4900		Cenomanian		OMV
Haidenbach-1	3019	3023.5	Santonian		RAG
Mank-1	157	oil stains	Eggenburgian		OMV
Northern Calcareous Alps (Austria)					
Urmannsau-1	152	oil stains	Allgäu Fm.		OMV
Urmannsau-1	758	oil stains	Wetterstein Fm.		OMV
Autochthnous Mesozoic (Austria)					
Kronberg-T1	4445	oil stains	Doggerian (Gresten Fm.)		OMV
Kronberg-T1	4680	oil stains	Doggerian (Gresten Fm.)		OMV
Klement-1	3537.5	3542.5	Doggerian (Gresten Fm.)		OMV
Various (Czech Republic)					
Cz.1	c.2400		Badenian		Vienna Basin

3. METHODS

Sediment samples were extracted for approximately 1 h using dichloromethane in a Dionex ASE 200 accelerated solvent extractor at 75°C and $5x10^6$ Pa. After evaporation of the solvent to 1 ml total solution in a Zymark TurboVap 500 closed cell concentrator, asphaltenes were precipitated from a hexane:dichloromethane solution (80:1) and separated by centrifugation. Oil samples (ca. 50 mg) were directly diluted with the hexane:dichloromethane (80:1) mixture and the insoluble asphaltenes were separated by centrifugation. The fractions of the hexane soluble organic matter were separated into polar compounds, saturated hydrocarbons and aromatic hydrocarbons by medium pressure liquid chromatography using a Köhnen–Willsch MPLC instrument (Radke et al., 1980).

Gas-Chromatography - Mass-Spectroscopy

The saturated and aromatic hydrocarbon fractions were analysed with a gas chromatograph equipped with a 60 m DB-5MS fused silica capillary column (i.e. 0.25 mm; 0.25 µm film thickness) coupled to a ThermoFisher ISQ quadrupol mass spectrometer. The oven temperature was programmed from 40° to 310°C at 4°C min^{-1}, followed by an isothermal period of 30 min. Helium was used as carrier gas. The sample was injected splitless, with the injector temperature at 275°C. The spectrometer was operated in the EI (electron ionisation) mode over a scan range from m/z 50 to m/z 650 (0.5 s total scan time). Data were processed with a Xcalibur data system. Individual compounds were identified on the basis of retention time in the total ion current (TIC) chromatogram and comparison of the mass spectra with published data. Relative percentages and absolute concentrations of different compound groups in the saturated and aromatic hydrocarbon fractions were calculated using peak areas in the TIC chromatograms in relation to those of internal standards (deuteriated *n*-tetracosane and 1,1´-binaphthyl, respectively), or by integration of peak areas in appropriate mass chromatograms using response factors to correct for the intensities of the fragment ion used for quantification of the total ion abundance.

Isotopy

The n-alkanes were separated from branched/cyclic hydrocarbons by an improved 5 Å molecular sieve method (Grice et al., 2008) for the analysis of stable carbon isotope ratios on individual n-alkanes and isoprenoids. Stable C isotope measurements were made using a Trace GC-ultra gas chromatograph attached to the ThermoFisher Delta-V isotope ratio mass spectrometer (irMS) via a combustion and high temperature reduction interface, respectively (GC Isolink, ThermoFisher). The GC coupled to the irMS was equipped with a 30 m DB-5MS

fused silica capillary column (i.d. 0.25 mm; 0.25 lm film thickness). The oven temperature was programmed from 70–300°C at a rate of 4°C/min followed by an isothermal period of 15 min. Helium was used as carrier gas. The sample was injected splitless at 275°C. For calibration, a CO_2 standard gas was injected at the beginning and at the end of each analysis. Isotopic compositions are reported in the δ notation relative to the PDB standards. Analytical reproducibility (0.2‰ for $\delta^{13}C$) was controlled by repeated measurements of n-alkane standard mixes.

4. RESULTS and DISCUSSION

Biomarker data from most source rocks and oils have been presented in earlier publications. Additional data are summarized in the Appendix. Therefore, the present report focuses on isotope data. CSI data for n-alkanes and isoprenoids are summarized for rock samples in Tables 4 and 5 and for oil samples in Table 6.

Table 4: Isotope data from Cenozoic rock samples

Sample	Depth / Heigth (m)	*n*-C15	*n*-C16	*n*-C17	*n*-C18	*n*-C19	*n*-C20	*n*-C21	*n*-C22	*n*-C23	*n*-C24	*n*-C25	*n*-C26	*n*-C27	*n*-C28	*n*-C29	C_{16}-Isoprenoid	Nor-pristane	Pristane	Phytane
Well A	2133.57	-28.5	-29.0	-29.4	-29.6	-30.0	-30.4	-31.0	-30.7	-30.5	-30.2	-29.9	-29.4	-29.1	-28.7	-28.8				
Well A	2136.15	-28.9	-29.1	-29.6	-29.9	-30.4	-31.0	-31.4	-31.3	-31.0	-30.8	-30.4	-29.9	-29.6	-29.2	-29.3				
Well A	2137.45	-28.4	-29.1	-29.5	-30.1	-30.4	-31.1	-31.6	-31.4	-30.9	-30.8	-30.3	-29.8	-29.5	-29.1	-29.4				
Well A	2138.50	-28.9	-29.2	-29.8	-29.7	-30.1	-30.8	-31.5	-31.1	-30.7	-30.6	-30.2	-29.7	-29.4	-29.1	-29.3				
Well C	2449.87	-28.1	-28.3	-28.9	-29.4	-30.0	-30.4	-30.9	-30.7	-30.2	-29.7	-29.2	-28.8	-28.6	-28.3	-28.4				
Well C	2451.27	-27.5	-27.9	-28.4	-28.8	-29.4	-30.0	-30.7	-30.5	-30.0	-29.6	-29.2	-29.0	-28.6	-28.3	-28.1				
Well C	2452.5	-27.7	-27.8	-28.8	-29.2	-29.7	-30.3	-31.0	-30.8	-30.4	-29.8	-29.3	-28.8	-28.5	-28.3	-28.1				
Hier-4	2400		-29.1	-29.6	-29.9	-30.1	-30.4	-30.6	-30.8	-31.2	-31.4	-31.8	-31.5	-31.7	-31.3	-31.8		-29.8	-30.5	-31.1
Hier-4	2420	-29.6	-30.1	-30.6	-30.9	-31.1	-31.4	-31.6	-31.5	-31.7	-31.4	-31.6	-31.6	-31.7	-31.8	-31.6	-29.8	-30.4	-31.3	-31.6
Hier-4	2425	-29.5	-30.0	-30.6	-31.1	-31.2	-31.4	-31.7	-31.6	-31.5	-31.3	-31.5	-31.6	-31.5	-31.3	-31.4	-29.7	-30.3	-31.2	-31.8
Hier-4	2435		-29.8	-30.4	-30.8	-31.0	-31.3	-31.5	-31.6	-31.8	-31.5	-31.1	-31.2	-31.3	-31.1	-31.3		-30.5	-31.1	-31.5
Osch-1	1369.17	-29.7	-30.5	-30.7	-31.3	-31.4	-31.5	-31.5	-31.7	-31.5	-31.4	-31.7	-31.8	-31.4	-31.6	-31.5	-29.6	-30.5	-30.7	-31.1
Osch-1	1371.22	-29.5	-29.9	-30.5	-31.1	-31.0	-31.2	-31.3	-31.7	-31.4	-31.2	-31.5	-31.7	-31.6	-31.4	-31.4	-29.7	-30.2	-31.0	-31.7
Osch-1	1373.29		-29.8	-30.9	-31.3	-31.7	-31.8	-31.6	-31.5	-31.0	-30.7	-30.7	-30.2	-29.8	-29.5	-29.6		-30.5	-31.3	-31.4
Osch-1	1375.82	-29.3	-29.4	-29.6	-30.2	-30.8	-31.1	-31.3	-30.9	-30.9	-30.3	-30.1	-29.8	-29.7	-29.8	-29.9		-30.1	-30.8	-31.2
Osch-1	1377.28	-28.8	-29.4	-29.8	-30.4	-30.7	-30.9	-31.2	-31.0	-30.8	-30.5	-30.3	-29.9	-29.6	-29.8	-29.9		-29.9	-30.7	-31.1
Osch-1	1379.9	-29.4	-30.2	-30.8	-31.0	-31.6	-31.9	-32.4	-31.7	-31.2	-30.8	-30.5	-30.3	-29.9	-29.7	-29.8	-30.2	-30.8	-31.0	-31.6
Osch-1	1381.79	-29.5	-30.3	-30.7	-31.2	-31.8	-32.0	-32.7	-31.8	-31.5	-31.1	-30.6	-30.2	-29.8	-29.7	-29.9	-29.7	-30.3	-30.9	-31.2
Osch-1	1382.05	-29.6	-29.9	-30.5	-30.9	-31.4	-32.1	-32.9	-31.6	-31.3	-30.9	-30.7	-30.1	-29.8	-29.6	-29.4	-29.9	-30.5	-30.9	-31.4
Osch-1	1382.49	-29.7	-30.1	-30.6	-31.2	-31.7	-31.9	-32.5	-31.5	-30.9	-30.5	-30.3	-29.9	-29.6	-29.4	-29.6	-30.1	-30.6	-31.4	-31.7
Osch-1	1383.96	-29.5	-29.6	-30.7	-31.3	-31.5	-32.2	-32.6	-31.7	-31.3	-30.8	-30.4	-29.7	-29.5	-29.7	-29.5	-29.6	-30.7	-31.3	-31.5
Osch-1	1384.46		-30.0	-30.4	-31.1	-31.6	-31.9	-32.7	-31.4	-31.2	-30.7	-30.5	-29.8	-29.7	-29.8	-29.5		-30.4	-31.2	-31.5
Osch-1	1385.45	-29.4	-30.4	-31.0	-31.6	-31.8	-31.8	-32.5	-31.7	-31.3	-30.9	-30.7	-30.1	-29.8	-29.6	-29.7	-29.8	-30.7	-31.1	-30.9
Osch-1	1387.7	-29.5	-29.9	-30.6	-31.0	-31.4	-32.0	-32.7	-31.6	-31.3	-30.9	-30.6	-30.1	-29.8	-29.6	-29.6	-30.1	-30.7	-31.4	-31.7
Osch-1	1389.24	-29.8	-30.2	-30.5	-31.0	-31.6	-31.7	-32.4	-31.5	-31.2	-30.8	-30.5	-30.3	-29.9	-29.7	-29.8	-29.9	-30.5	-31.0	-31.4
Osch-1	1390.75		-30.1	-30.4	-30.9	-31.6	-31.9	-32.5	-31.4	-31.2	-30.8	-30.4	-29.9	-29.6	-29.8	-29.5		-30.4	-31.3	-31.6
Osch-1	1392.87		-30.3	-30.9	-31.3	-31.7	-31.9	-32.6	-31.5	-31.4	-31.1	-30.7	-30.2	-30.0	-29.7	-29.9		-30.3	-30.9	-31.4
BHN-2	1865.48		-27.0	-27.6	-27.5	-27.4	-27.7	-27.9	-28.4	-28.7	-28.8	-29.5	-29.4	-29.3	-29.1	-29.5			-28.5	-28.9
BHN-2	1866.78		-26.8	-27.4	-27.2	-27.3	-27.5	-27.6	-28.3	-28.5	-28.6	-29.3	-29.5	-29.2	-28.9	-29.6			-28.4	-28.6
Molln-1	5190	-30.4	-30.6	-31.2	-32.0	-32.6	-32.7	-32.8	-32.0	-31.6	-31.7	-31.3	-30.9	-30.6					-31.3	-31.9
Molln-1	5200	-30.3	-31.2	-31.5	-32.3	-32.6	-32.2	-32.9	-32.4	-31.9	-31.6	-31.1	-30.7	-30.5					-31.4	-32.1
Obhf-1 (545)	4293	-28.3	-29.4	-29.8	-30.3	-30.6	-30.9	-31.7	-31.4	-31.2	-30.4	-30.4	-29.9						-29.9	-30.3
Obhf-1 (540)	4295	-28.6	-29.3	-29.7	-30.3	-30.5	-31.1	-31.5	-31.4	-31.2	-30.6	-30.6	-29.8						-29.8	-30.4
Thomasl-1	1650	-28.3	-28.5	-28.6	-28.7	-28.9	-28.8	-29.0	-28.5	-28.8	-29.3	-29.0	-29.4	-29.3	-29.7			-28.3	-28.5	-28.6
Thomasl-1	1720	-28.3	-28.0	-28.3	-28.1	-28.3	-28.5	-29.0	-28.6	-28.9	-29.0	-29.2	-29.4	-29.5	-29.9			-28.3	-28.0	-28.3
Thomasl-1	1760	-28.2	-28.3	-28.3	-28.3	-28.4	-28.7	-29.1	-28.9	-29.0	-29.1	-29.4	-29.6	-29.4	-30.1	-29.8		-28.2	-28.3	-28.3

Table 5: Isotope data from Mesozoic rock samples

Sample	**Depth (m)**	*n*-C15	*n*-C16	*n*-C17	*n*-C18	*n*-C19	*n*-C20	*n*-C21	*n*-C22	*n*-C23	*n*-C24	*n*-C25	*n*-C26	*n*-C27	*n*-C28	*n*-C29	C_{16}-Isoprenoid	Nor-pristane	Pristane	Phytane
Mistelgau					-28.6	-29.0	-28.9	-28.8	-28.9	-29.2	-29.3	-29.8	-29.3	-29.5	-29.0	-29.8			-28.9	-29.4
Dotternhausen		-30.7	-32.3	-31.9	-32.8	-33.5	-33.7	-33.6	-33.7	-34.1	-34.2	-34.4	-34.2	-34.5			-30.9	-31.8	-32.5	-33.1
Schönlind; H				-29.1	-29.3	-29.3	-29.4	-29.4	-29.2	-29.6	-29.7	-30.0	-29.7	-29.9					-29.5	-29.8
Schönlind; S				-28.8	-29.1	-29.4	-29.4	-29.2	-29.3	-29.7	-29.8	-30.2	-29.8	-30.0	-29.6	-30.0			-29.4	-29.7
Bächental (35)			-31.5	-31.8	-32.1	-32.3	-32.5	-31.9	-31.8	-31.6	-31.0	-30.6	-30.3	-30.2			-31.6	-31.8	-32.0	-32.3
Bächental (26)				-31.4	-31.7	-32.2	-32.3	-32.0	-31.7	-31.5	-31.2	-30.8	-30.6	-30.5				-31.6	-31.9	-32.4
Bächental (25)			-31.3	-31.5	-31.8	-32.1	-31.9	-31.6	-31.7	-31.3	-30.8	-30.7	-30.5	-30.3			-31.2	-31.5	-31.8	-32.2
Falkenst.-KB-4				-32.8	-32.5	-32.8	-32.7	-32.6	-32.8	-32.7	-32.7	-32.9	-33.0	-32.6	-32.8			-32.9	-32.6	-33.0
Falkenst.-KB-5			-32.1	-32.6	-32.6	-32.7	-32.5	-32.7	-32.8	-32.5	-32.7	-33.2	-32.6	-32.4	-32.5	-32.2	-32.4	-32.6	-32.8	-32.9
Falkenst.-KB-7				-32.2	-31.8	-32.0	-31.8	-32.1	-32.2	-32.4	-33.0	-32.7	-32.8	-32.3	-32.4			-32.2	-31.9	-32.2
Witzala APII 1		-27.2	-27.5	-27.7	-27.4	-27.8	-27.6	-27.9	-28.0	-27.7	-27.9	-27.7	-27.9	-28.2	-28.1	-28.3	-27.4	-27.9	-28.0	-28.2
Witzala APII 4		-26.5	-26.7	-26.7	-26.9	-27.0	-27.1	-27.3	-26.9	-26.7	-26.8	-26.9	-27.3	-27.5			-27.1	-27.5	-27.9	-28.0
Witzala APII 6		-26.2	-26.6	-26.7	-27.1	-27.3	-27.4	-27.5	-27.8	-27.6	-27.7	-27.8	-28.0	-28.3	-28.1	-28.4	-26.9	-27.2	-27.6	-27.6
Witzala APII 10		-27.1	-27.2	-27.5	-27.7	-27.6	-27.9	-28.0	-27.9	-27.7	-27.8	-28.1	-27.9	-28.2	-28.0	-28.3	-27.0	-27.3	-27.7	-27.8
Witzala APII 20		-26.6	-26.9	-27.2	-27.0	-27.5	-27.8	-27.6	-27.4	-27.6	-27.3	-27.7	-27.7	-28.1	-27.8	-28.2	-27.3	-27.5	-27.9	-28.1
Witzala APII 26		-26.7	-26.9	-26.7	-27.1	-27.2	-27.0	-27.3	-26.9	-27.2	-27.3	-27.3	-27.6	-28.1	-27.7	-28.0	-26.9	-27.4	-27.5	-27.7
Witzala APII 37		-26.3	-26.7	-26.4	-27.0	-26.7	-26.6	-26.5	-26.6	-26.8	-27.0	-27.3	-27.5	-28.0	-27.9	-28.1	-26.3	-26.6	-26.9	-27.2
Witzala APII 44		-26.8	-27.1	-27.2	-27.3	-27.5	-27.2	-27.5	-27.6	-27.9	-27.9	-28.3	-27.8	-28.1	-27.9	-28.3	-26.8	-27.2	-27.6	-27.7
Witzala APII 48			-27.1	-26.9	-27.1	-27.2	-27.3	-27.5	-27.7	-27.6	-27.8	-27.7	-27.9	-28.2	-27.7	-28.2		-27.5	-27.8	-27.8
Witzala APII 49			-26.2	-26.4	-26.7	-26.6	-27.0	-27.0	-27.3	-27.0	-27.3	-27.5	-27.7	-27.9	-27.8			-27.0	-27.4	-27.7
Witzala APII 52			-27.0	-27.1	-27.3	-27.5	-27.8	-27.7	-27.5	-27.6	-27.4	-27.9	-27.8	-28.1	-27.8			-27.8	-28.0	-28.3
Witzala APII 53			-27.4	-27.6	-27.7	-27.6	-27.7	-27.8	-27.7	-27.6	-27.9	-28.1	-27.9	-28.0	-27.9			-27.8	-28.1	-28.3
Zistersdorf-ÜT1	5605.5		-30.3	-28.8	-29.4	-29.2	-29.5	-29.8	-29.3	-29.2	-28.5								-34.2	-33.6
Zistersdorf-ÜT1	5740.7	-29.8	-29.7	-31.3	-33.5	-33.4	-32.7	-31.9	-31.7	-31.6	-31.0	-31.9	-30.7	-31.9	-31.5				-35.5	-33.4
Maustrenk-ÜT1	6546.7			-29.3	-28.6	-28.3	-28.5	-29.0	-27.7											
Maustrenk-ÜT1	6548.8	-30.4	-29.9	-29.6	-30.0	-30.0	-30.5	-30.7	-30.5	-30.4	-30.4	-30.7	-30.3	-30.8	-31.2				-39.1	-33.8

Table 6: Isotope data from oil samples

Sample	*n*-C15	*n*-C16	*n*-C17	*n*-C18	*n*-C19	*n*-C20	*n*-C21	*n*-C22	*n*-C23	*n*-C24	*n*-C25	*n*-C26	*n*-C27	*n*-C28	*n*-C29	*n*-C30	*n*-C31	C_{16}-Isoprenoid	Nor-pristane	Pristane	Phytane
Molasse Basin																					
Kohleck-2	-28.5	-28.9	-29.4	-29.8	-30.4	-31.5	-32.2	-30.4	-30.4	-29.2	-29.1	-29.1	-29.4	-28.9	-29.2	-29.4	-29.3				
Kemating-W2	-29.1	-29.5	-30.1	-30.3	-30.8	-31.3	-31.7	-31.6	-32.1	-31.9	-31.3	-30.4	-30.6	-30.0	-29.4						
Kemating-1	-28.2	-29.1	-29.5	-30.1	-30.4	-31.0	-31.6	-31.7	-31.6	-30.4	-30.6	-30.5	-30.2	-29.7	-30.4						
M. Schmolln-1	-28.8	-28.9	-29.9	-29.9	-30.5	-30.7	-32.1	-31.6	-31.5	-30.0	-29.4	-29.9	-29.6	-29.4	-28.6	-28.3	-28.4				
Steindlberg-1	-28.3	-28.8	-29.7	-29.9	-31.2	-31.7	-32.5	-31.8	-31.6	-29.9	-29.8	-29.6	-29.5	-28.7	-28.5	-28.5	-28.7				
Steindlberg-2	-28.6	-29.1	-29.6	-30.2	-30.7	-31.1	-31.6	-31.5	-31.8	-31.5	-31.1										
Ried-5	-29.5	-29.9	-30.1	-30.6	-30.9	-31.3	-31.9	-31.3	-31.5	-30.3	-30.5	-30.3	-30.1	-30.1	-29.6	-29.6	-29.3				
Trat 7	-30.7	-30.4	-31.5	-31.4	-31.7	-31.9	-32.9	-31.2	-31.1	-29.4	-29.5	-29.3	-29.8	-29.2	-29.9	-29.2	-29.6				
Trat 8	-29.0	-29.6	-29.6	-30.3	-30.4	-31.0	-32.9	-31.5	-31.2	-30.7	-29.9	-29.3	-29.5	-28.2	-29.5	-29.3	-28.4				
Trat 10	-28.7	-29.2	-30.2	-30.0	-30.8	-31.7	-32.8	-31.9	-32.3	-30.1	-30.2	-29.7	-29.8	-29.6	-30.1	-29.3	-28.4				
Puchkirchen-1	-29.4	-29.7	-30.3	-30.7	-31.4	-31.2	-31.9	-30.9	-30.7	-30.1	-30.0	-30.0	-30.3	-30.2	-30.3	-29.9	-30.1				
Schwanenstadt-2	-28.5	-29.1	-30.0	-30.3	-31.5	-31.7	-33.0	-31.3	-31.7	-30.6	-30.2	-29.7	-29.7	-29.0	-29.3	-29.2					
Wegscheid-1	-29.5	-29.7	-30.4	-30.8	-31.5	-31.6	-32.1	-33.2	-32.6	-32.0	-31.5	-30.8	-30.6	-30.2	-29.6	-29.4	-29.1				
Lindach-1	-28.8	-29.6	-30.1	-30.2	-30.8	-32.1	-32.8	-33.3	-32.5	-31.5	-30.7	-29.9	-29.8	-29.0	-29.6	-29.3	-28.6				
Mühlreith 3257	-29.0	-29.0	-30.4	-30.1	-31.0	-31.4	-32.3	-31.7	-31.6	-31.5	-31.2	-30.4	-30.2	-29.5	-29.8	-30.0	-29.5				
BH 2	-30.5	-30.3	-31.3	-31.6	-32.7	-32.7	-33.9	-32.1	-32.0	-31.0	-30.6	-30.0	-30.7	-29.8	-30.9	-30.1	-29.2				
BH 9	-30.6	-30.5	-30.9	-31.2	-31.8	-32.3	-32.8	-32.4	-32.4	-31.8	-31.3	-31.0	-30.5	-30.2	-30.6						
BH N1	-29.2	-29.6	-30.9	-30.5	-31.5	-32.2	-34.0	-32.5	-32.2	-32.1	-31.5	-31.1	-30.8	-30.1	-30.7	-30.6	-29.5				
BH 7	-29.9	-30.3	-30.9	-30.8	-31.8	-31.9	-32.5	-32.6	-32.5	-31.2	-30.8	-30.3	-29.8	-29.8	-30.0	-28.9	-29.7				
Kematen-1	-31.4	-32.1	-32.2	-32.6	-33.3	-33.5	-34.8	-32.8	-33.2	-30.7	-31.8										
Engenfeld-1	-28.8	-29.5	-30.5	-31.7	-32.1	-32.5	-33.2	-33.9	-32.3	-31.8	-31.4	-30.6	-29.6	-28.6	-29.4	-29.0	-29.4				
Engenfeld-6	-31.6	-31.3	-31.4	-32.0	-32.5	-32.2	-33.8	-31.9	-32.2	-30.3	-30.6										
Piberbach-7	-29.6	-30.3	-30.8	-31.3	-31.6	-32.3	-32.7	-33.1	-32.6	-32.2	-31.5	-31.1	-30.5	-30.2							
Pfarrkirchen-1	-29.9	-30.0	-30.6	-31.5	-32.3	-32.3	-33.6	-32.8	-32.5	-31.7	-30.5	-30.2	-30.8	-29.9	-30.3	-29.4	-29.9				
Mdf	-30.9	-31.4	-31.7	-32.8	-34.0	-33.4	-34.9	-32.8	-33.4	-33.2	-32.9	-32.5									
Eberstalzell-2a	-29.7	-29.3	-29.6	-31.0	-33.1	-33.9	-35.3	-34.4	-34.8	-31.9	-31.4	-30.5	-30.7	-29.6	-29.6	-29.2	-28.8				
Eberstalzell-6	-29.4	-30.8	-31.1	-31.3	-32.0	-32.1	-33.4	-32.5	-32.2	-30.1	-29.5	-29.1	-29.5	-28.7	-29.4	-29.3	-29.0				
Eberstalzell-7	-30.1	-30.3	-30.7	-31.2	-31.7	-31.9	-33.2	-31.6	-31.6	-30.7	-30.3	-29.9	-30.2	-30.0	-30.0	-28.9	-29.4				
Oberaustall-1	-30.0	-31.2	-31.6	-32.2	-32.2	-32.2	-33.2	-31.3	-30.9	-29.9	-29.3	-28.9	-29.3	-29.0	-29.2	-28.5	-28.9				
Oberaustall-1	-30.1	-29.7	-30.4	-29.9	-29.3	-29.7	-31.2	-30.7	-30.5	-30.2	-29.7	-29.2	-30.3								
Oberaustall-2	-29.4	-29.7	-30.2	-30.6	-32.6	-32.8	-33.7	-31.5	-31.4	-30.2	-29.8	-29.0	-29.9	-28.4	-29.4	-29.5	-28.4				
Sattledt-2	-30.1	-31.2	-31.1	-32.5	-32.7	-32.4	-33.5	-32.0	-32.3	-31.4	-30.9	-30.8	-29.7	-29.5	-29.6						
Sattledt-10	-29.8	-28.6	-29.7	-30.2	-32.4	-32.0	-32.7	-31.4	-31.2	-30.0	-30.0	-30.5	-29.6	-29.1	-29.1						
Sattledt-23	-28.6	-28.5	-29.5	-30.3	-30.8	-32.0	-33.3	-32.6	-31.6	-29.5	-28.8	-29.2	-29.4	-28.6	-28.0	-28.2	-28.3				
Rappersdorf-2	-29.6	-29.7	-29.9	-30.8	-32.2	-32.9	-35.1	-33.2	-33.1	-31.8	-30.3	-29.9	-30.1	-29.5							
Steinhaus-6	-29.8	-30.8	-31.3	-32.1	-32.0	-31.8	-31.7	-31.5	-30.8	-30.9	-31.2	-30.4	-30.7	-29.7	-30.3	-29.7					
Steinhaus-N2	-28.8	-29.5	-30.1	-31.1	-33.3	-32.3	-33.8	-32.0	-33.4	-31.6											
Wels N1	-29.7	-30.1	-30.4	-30.5	-30.8	-31.3	-31.6	-31.5	-31.5	-31.0	-30.7	-30.2	-30.6	-29.9	-30.2	-29.7	-29.2				

Table 6: Isotope data from oil samples (continued)

Sample	*n*-C15	*n*-C16	*n*-C17	*n*-C18	*n*-C19	*n*-C20	*n*-C21	*n*-C22	*n*-C23	*n*-C24	*n*-C25	*n*-C26	*n*-C27	*n*-C28	*n*-C29	*n*-C30	*n*-C31	C_{16}-Isoprenoid	Nor-pristane	Pristane	Phytane
Vo 13	-29.4	-29.8	-30.3	-31.8	-32.3	-32.4	-33.5	-32.0	-32.0	-30.1	-30.5	-29.6	-30.1	-30.4	-30.1	-30.0	-29.3				
Vo 19	-31.1	-30.6	-31.1	-31.6	-32.6	-32.8	-34.1	-32.7	-32.9	-32.2	-31.9	-31.4	-31.8	-31.6	-31.5						
Vo 23	-30.9	-31.0	-31.2	-32.0	-32.5	-32.7	-33.6	-32.2	-32.6	-31.8	-32.1	-31.9									
Vo 41	-29.9	-29.7	-30.2	-30.5	-31.4	-31.8	-33.1	-31.3	-31.2	-29.8	-29.5	-29.3	-29.5	-28.9	-29.0	-28.9	-28.9				
V-01	-29.8	-30.0	-30.9	-31.2	-32.2	-32.2	-33.1	-31.7	-31.7	-31.0	-30.9	-30.6	-30.4	-30.2	-30.8			-29.9	-30.1	-30.8	-31.3
V-02	-30.1	-30.4	-31.1	-31.6	-32.5	-32.3	-33.3	-31.8	-31.7	-30.9	-30.8	-30.5	-30.3	-30.8	-31.1			-30.2	-30.5	-31.2	-31.7
V-08	-30.7	-30.7	-31.2	-31.5	-32.4	-32.3	-33.3	-31.8	-31.4	-31.0	-30.7	-31.0	-30.4	-30.7	-30.9			-30.9	-31.0	-31.3	-31.5
V-11	-30.0	-31.0	-31.3	-31.3	-32.3	-32.1	-32.9	-31.6	-31.6	-30.8	-31.0	-30.4	-30.9	-31.1	-31.2			-30.2	-31.1	-31.4	-31.4
V-13	-30.2	-30.5	-31.0	-31.6	-32.3	-32.3	-33.4	-31.9	-31.7	-31.1	-31.0	-30.7	-30.7	-30.4	-30.9			-30.3	-30.6	-30.9	-31.5
V-15	-30.0	-30.9	-31.4	-31.7	-32.4	-32.7	-33.3	-31.6	-31.8	-30.9	-30.7	-30.6	-30.9	-30.4	-30.7			-30.1	-30.7	-31.4	-31.8
V-19	-30.2	-30.3	-31.0	-31.4	-32.5	-32.2	-33.3	-31.7	-31.9	-31.1	-31.0	-30.5	-30.6	-30.7	-30.9			-30.3	-30.4	-31.0	-31.6
V-21	-29.7	-30.1	-30.8	-31.4	-32.5	-32.3	-33.6	-31.8	-31.9	-31.1	-31.1	-30.3	-30.6	-30.5	-30.7			-29.8	-30.2	-30.7	-31.4
V-23	-30.0	-30.1	-31.0	-31.6	-32.5	-32.5	-33.6	-32.1	-31.8	-31.0	-30.9	-30.9	-30.7	-30.3	-31.1			-30.1	-30.3	-30.9	-31.5
V-33	-29.9	-30.0	-30.9	-31.6	-32.7	-32.6	-33.6	-32.3	-31.9	-31.1	-31.2	-30.2	-30.9	-30.1	-31.0			-29.8	-30.1	-30.8	-31.6
V-39	-30.0	-30.1	-31.1	-31.7	-32.8	-32.6	-33.6	-32.1	-32.0	-30.9	-30.9	-30.6	-30.7	-30.3	-31.1			-30.1	-30.3	-31.0	-31.7
V-41	-30.2	-30.3	-31.2	-31.7	-32.9	-33.0	-33.7	-31.9	-31.9	-31.0	-31.1	-30.8	-31.2	-30.7	-31.1			-30.3	-30.4	-31.3	-31.7
Sierning-1	-30.8	-31.3	-30.8	-31.5	-31.8	-32.4	-32.8	-33.2	-32.6	-32.1	-31.6	-31.1	-30.5	-29.8	-29.9	-29.5	-29.3				
Wirnzberg-1	-30.5	-30.9	-31.1	-31.6	-32.3	-32.7	-33.2	-32.9	-32.4	-31.8	-31.3	-30.8	-30.6	-30.1	-30.4	-30.2	-29.7				
Gruenau-1	-29.7	-30.1	-31.7	-31.7	-32.5	-32.3	-33.3	-32.7	-32.7	-31.8	-32.1	-31.3	-31.8	-31.4	-30.7						
Haidenbach-1	-29.5	-29.6	-30.0	-30.6	-31.3	-31.5	-32.3	-31.4	-31.0	-30.6	-30.3	-30.3	-30.1	-29.7	-29.8				-29.8	-30.2	-30.7
Mank-1			-27.3	-27.5	-27.9	-28.0	-27.9	-28.1	-28.0	-28.2	-28.6	-28.8	-29.0	-28.9	-28.5				-27.2	-27.5	-27.9
Northern Calcareous Alps (Austria)																					
Urmannsau-1		-26.3	-26.6	-27.1	-27.3	-27.8	-28.2	-28.5	-28.8	-28.4	-28.8	-28.7	-28.6	-28.7	-29.1			-26.5	-26.7	-27.1	-27.4
Urmannsau-1			-26.8	-27.1	-27.2	-27.4	-27.6	-27.9	-28.2	-28.6	-28.7	-28.5	-28.6	-28.3	-28.5				-26.9	-27.1	-27.3
Autochthonous Mesozoic (Austria)																					
Kronberg-T1	-27.6	-27.7	-27.6	-27.9	-28.2	-28.4	-28.5	-28.6	-28.8	-28.9	-29.0	-28.9	-29.2	-29.3	-29.5			-28.1	-28.4	-28.7	-28.6
Kronberg-T1	-27.8	-28.4	-28.7	-29.1	-29.6	-29.7	-29.9	-30.1	-30.1	-30.3	-30.4							-28.3	-28.7	-29.1	-29.5
Klement-1	-27,0	-26,7	-26,4	-27,1	-27,5	-27,3	-27,4	-27,7	-27,4	-27,3	-27,4	-27,6	-27,9	-27,8	-28,0	-28,3					
Carpathians (Czech Rep.)																					
Cz-1	-27.4	-27.6	-28.1	-27.8	-27.7	-27.4	-27.9	-27.7	-27.7	-27.6	-27.8	-28.1	-28.0	-28.2	-27.6			-27.6	-27.9	-28.3	-28.1

4.1 Rock samples

4.1.1 Eocene and Oligocene rocks in the Austrian Molasse Basin

$\delta^{13}C$ ratios of n-alkanes of Eocene and Oligocene rocks in the Upper Austrian part of the Molasse Basin are plotted together with relative percentages of n-alkanes (derived from GC-FID) in Fig. 2. Mean values of isotope ratios are plotted in Fig. 3 versus chain length.

Upper Eocene Cerithian Beds are interpreted as brackish tidal flat deposits (Wagner, 1980, 1998) and contain dark-grey fossiliferous mudstones with a very good oil potential (up to 6 % TOC, HI: 550 mgHC/gTOC; Table 1). Extracts from these rocks are characterized by relatively high $\delta^{13}C$ ratios and a decrease in $\delta^{13}C$ with increasing chain length (Figs. 2, 3).

The Lower Oligocene deep-water succession includes the most important source rocks in the Molasse Basin (Schöneck Fm., Eggerding Fm.; Schulz et al., 2002; Sachsenhofer et al., 2010). Schulz et al. (2002) subdivided the Schöneck Formation (nannoplankton zones NP21, NP22) into the marly units "a" and "b" and the shaly unit "c". The overlying Dynow Formation represents the brackish-water "Solenovian Event" (lower part of NP23; Sachsenhofer et al., 2018a,b). Rock extracts from the Schöneck and Dynow formations are characterized by very specific V-shaped CSI patterns (Figs. 2, 3), which result from very low $\delta^{13}C$ values of medium-chain length n-alkanes (minimum at C_{21}). This is also valid for samples from the Oberhofen and Molln wells, which are not precisely dated (Table 4).

The Eggerding and Zupfing formations (Sachsenhofer et al., 2010) follow above the Dynow Formation, but do not show the V-shaped CSI pattern. This is because medium-chain n-alkanes are heavier, while long-chain n-alkanes are lighter than in the underlying units. This is also evident in Fig. 4, where isotope ratios of n-C_{16}, n-C_{21} and n-C_{29} are plotted versus stratigraphy (using the stratigraphy of borehole Osch-1).

Several important trends become visible:

- Isotope ratios of Eocene rocks are significantly higher than those of Oligocene rocks.
- Within the Oligocene section, isotope ratios of short-chain n-alkanes, pristane and phytane show little variability.
- In contrast, medium-chain n-alkanes are very light in the lower part of the Oligocene section and get heavier within the Dynow Formation.
- Long-chain n-alkanes are uniform across the Eocene/Oligocene boundary, but show a shift towards lighter $\delta^{13}C$ ratios at the top of the Dynow Formation.

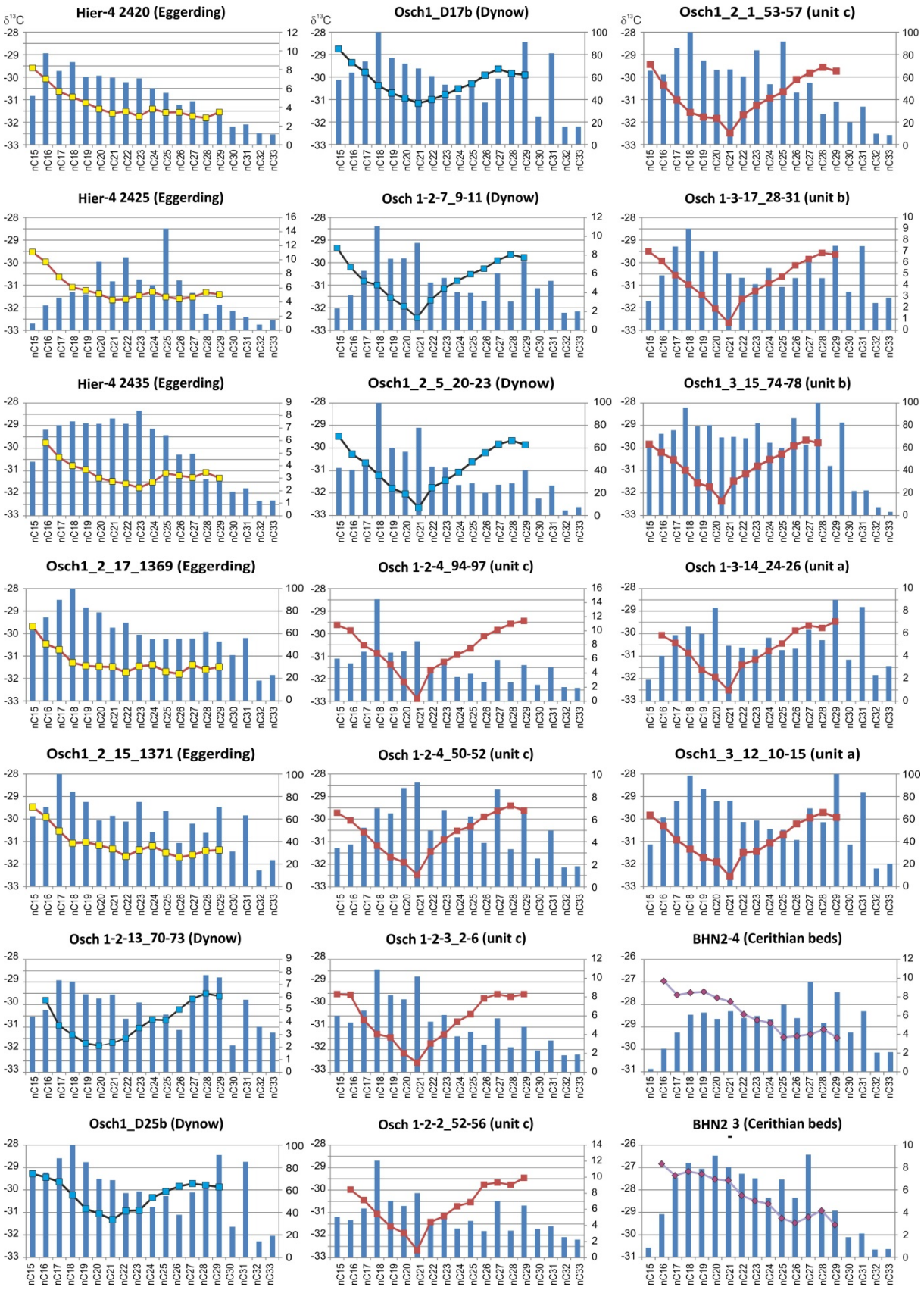

Fig. 2. Isotope ratios and relative abundance of n-alkanes in rock extracts from Upper Eocene (Cerithian Beds) and Lower Oligocene units in Upper Austria.

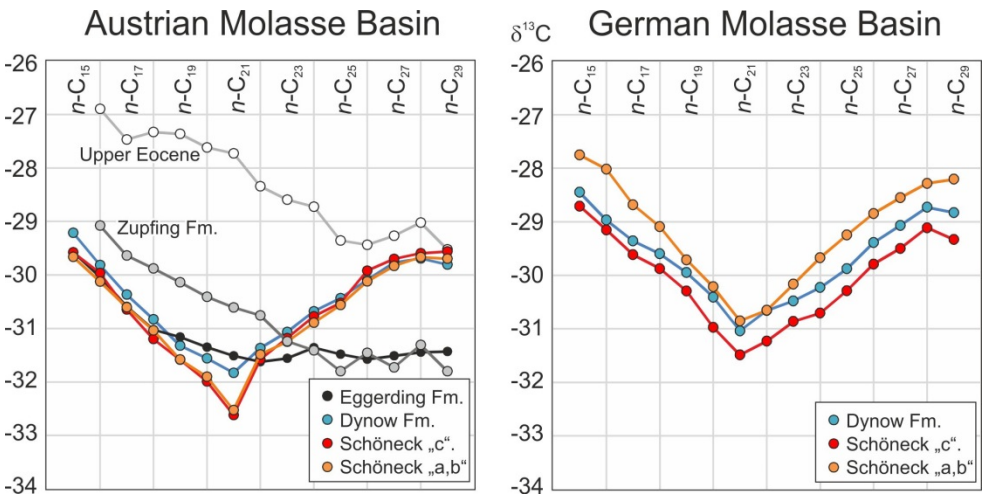

Fig. 3. Carbon isotopic composition ($\delta^{13}C$) of individual n-alkanes. Shown are mean values for different stratigraphic units in the Austrian and German parts of the Molasse Basin.

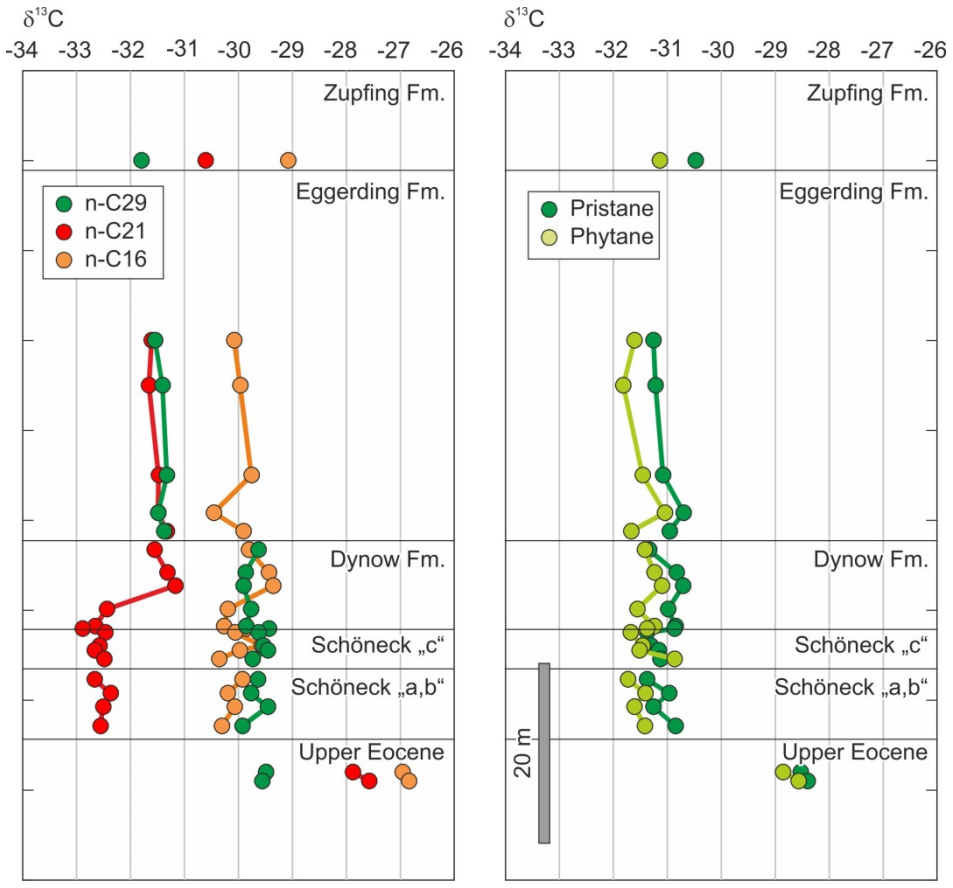

Fig. 4: Depth plot of $\delta^{13}C$ ratios of short (C_{16}), middle (C_{21}) and long-chain n-alkanes (C_{29}). Isotope ratios for pristane and phytane, derived from chlorophyll, are shown for comparison. Data are from different wells.

Carbon isotope ratios of organic matter depend on a variety of factors including the relative contributions of aquatic and terrestrial organic matter, the relative contributions of C3 and C4 land plants, temperature, maturity, etc. (e.g. Hoefs, 2009). Hence, currently it is impossible to explain the observed trends. Nevertheless, the authors dare to attempt some explanations:

Long-chain n-alkanes (e.g. n-C_{29}) are often considered to be derived from higher land plants (mainly plant waxes; Eglinton and Hamilton, 1967). However algae and submerged plants also can contribute to them (e.g. Lichtfouse et al., 1994; Liu and Liu, 2016). $\delta^{13}C$ ratios are constant across the Eocene/Oligocene boundary, but a 2 ‰ negative shift occurs at the top of the Dynow Formation, which is difficult to explain, if only a terrestrial source is considered.

Middle chain n-alkanes (e.g. n-C_{21}) may originate from aquatic macrophytes (Ficken et al., 2000), but essentially their origin is largely speculative. They are characterized by high ratios in Upper Eocene rocks, a major negative 5 ‰ shift at the base of the Schöneck Formation and a moderate positive (1 ‰) shift within the Dynow Formation. Interestingly, the positive shift of n-C_{16} predates the negative shift of n-C_{29}.

Short chain n-alkanes (n-C_{16}) are typically attributed to aquatic, algal organisms. In the studied section, n-C_{16} is isotopically heavy in the Upper Eocene and remains largely constant in the overlying units. Slightly higher values are observed near the base of the Zupfing Formation. We speculate that the relatively high $\delta^{13}C$ ratios in the Upper Eocene Cerithian Beds reflect higher temperatures due to a shallow depositional environment.

Pristane and phytane are diagenetic products of chlorophyll present both in terrestrial and aquatic plants. Overall their $\delta^{13}C$ trends are more similar to that of n-$C_{16,}$ than to that of n-C_{29}. This may indicate that pristane and phytane are mainly derived from aquatic organisms. Alternatively, high ratios in the shallow-water Cerithian Beds may reflect a higher contribution of land plants. This interpretation is supported by $\delta^{13}C$ values of Lower Upper Eocene and Lower Oligocene coals and wood, which typically range from -24 to -26 ‰ (Bechtel et al., 2008).

Irrespective of the biological and environmental controls on varying isotope ratios, the stratigraphy-dependant values allow very detailed oil-source correlations.

4.1.2 Oligocene rocks in the German Molasse Basin

Seven samples from the German part of the Molasse Basin have been investigated in order to test, if the V-shaped CSI pattern is a local phenomenon or characteristic for the entire Molasse Basin. Three samples represent the marly units "a/b" of the Schöneck Formation and are from the area east of Munich. These samples have a very low maturity (Tmax: ~416°C) despite of considerable depth (~2450 m). Four samples from shallower depth (~2350 m), but with higher maturity (Tmax ~432°C) are from a well west of Munich and represent the shaly unit "c" of the Schöneck Formation (3 samples) and the lower part of the Dynow Formation (1 sample).

Mean isotope ratios for each unit are plotted in Fig. 3. All units show the same V-shaped CSI patterns as in Upper Austria. This shows that the V-shape is characteristic for the Schöneck and Dynow formations in the entire Molasse Basin.

In contrast to Upper Austria, isotope ratios of the marly units "a/b" of the Schöneck Formation are higher than those of the shaly unit "c". However, a maturity effect cannot be excluded. Moreover, the distance of both wells is about 150 km.

4.1.3 Oligocene rocks in the Waschberg Zone

The Thomasl Formation in the Waschberg Zone is a time-equivalent to the Eggerding Formation in the Molasse Basin (Fuchs et al., 2001). In boreholes it holds a fair to good hydrocarbon potential (up to 3.7 % TOC; type III and type II kerogen) (Pupp et al., 2018).

Three cuttings samples from borehole Thomasl-1 are included in the present study (Table 1). Their CSI patterns are displayed in Fig. 4.

Similar to the coeval rocks of the Eggerding Formation in the Molasse Basin, the Thomasl Formation is characterized by decreasing $\delta^{13}C$ ratios with increasing chain length. However, the ratios are slightly higher than in the Molasse Basin. Maceral composition and relatively low HI values (Pupp et al., 2018) suggest that this reflects a higher contribution of land plants.

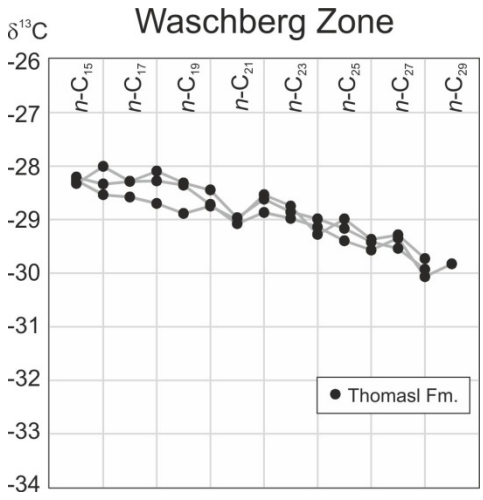

Fig. 4. Carbon isotopic composition ($\delta^{13}C$) of individual n-alkanes from rock extracts in the Thomasl Formation.

4.1.4 Mesozoic rocks in the Gailtal Alps

"Upper Hauptdolomite" is exposed NE of the Witzala Mountain in Carinthia (Fig. 1). Abram (2001) described two lithotypes: bright coarse-grained dolostone with single clay layers and black laminated, marly dolostone with high TOC contents. Migrated bitumen occurs in fractures and dissolution pores in the dolostones.

CSI patterns are displayed in Fig. 5. Despite of great differences in organic matter content (0.3-21.8 %TOC, Table 2), CSI patterns are similar. This suggests that the migrated bitumen was generated within the same unit.

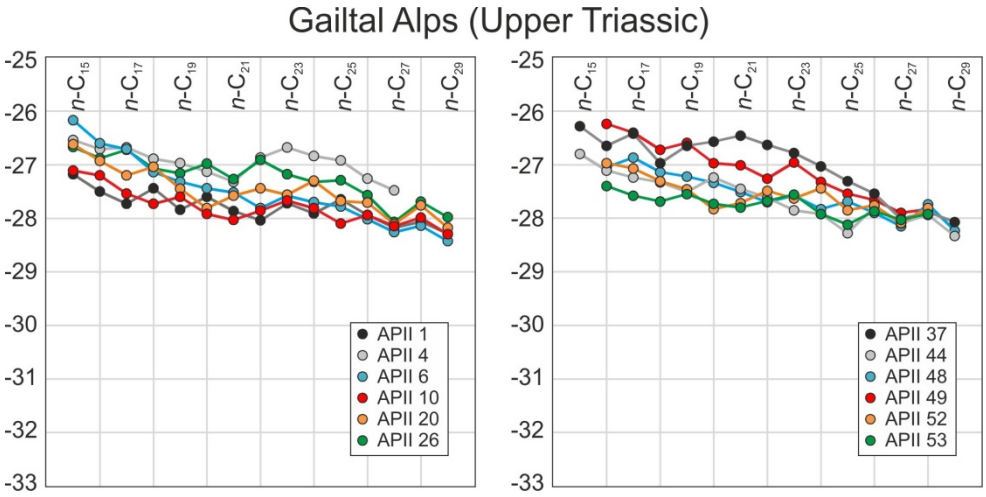

Fig. 5. Carbon isotopic composition ($\delta^{13}C$) of individual n-alkanes of Upper Triassic rocks in the Gailtal Alps.

4.1.5 Mesozoic rocks in the Northern Calcareous Alps

Mesozoic rocks in the Northern Calcareous Alps, including the Triassic Refiling Limestone (Gratzer et al., 2015 and the Toarcian Bächental Bituminous Marl (Neumeister et al., 2015), may generate oil, which may have charged structures within the Alpine nappe stack.

Fig. 6 shows that each of the investigated stratigraphic units is characterized by specific CSI patterns. Extracts from the Triassic Reifling Limestone contain n-alkanes with isotopically light carbon. The Toarcian Bächental Bituminous Marl shows a V-shaped with a minimum at C_{19}/C_{20}.

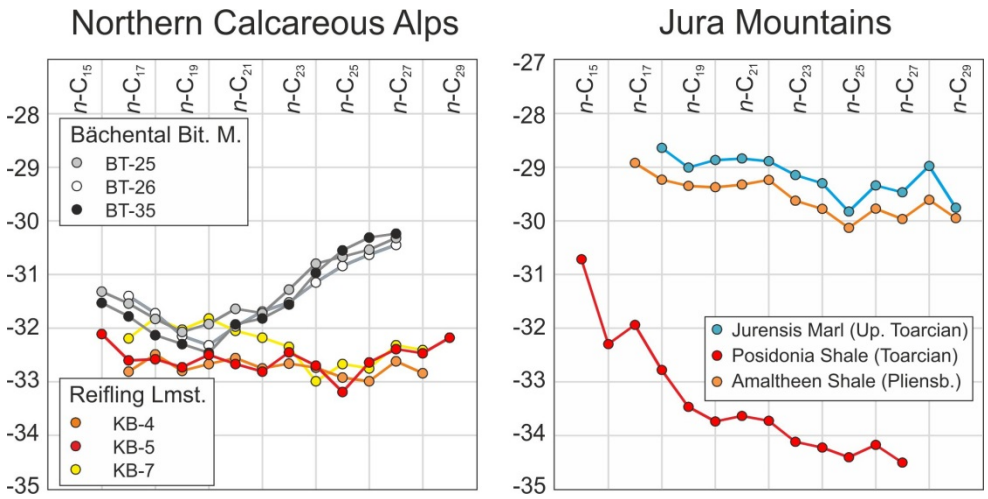

Fig. 6. Carbon isotopic composition ($\delta^{13}C$) of individual n-alkanes of Mesozoic rocks in the Calcareous Alps (Austria) and the Jura Mountains (Germany).

4.1.6 Mesozoic rocks in the Jura Mountains

Although located in Germany, Lower Jurassic rocks from the Jura Mountains are included in the study, in order to compare the Toarcian Bächental Bituminous Marl in the Calcareous Alps with coeval rocks (Posidonia Shale) and because Mesozoic rocks in the Jura Mountains continue southwards beneath the Molasse Basin and, therefore, may contribute to the accumulated oils (e.g. Wehner and Kuckelkorn, 1995).

Fig. 6 reveals major differences between the Bächental Bituminous Marl and the Posidonia Shale. In contrast to the isotopically very light Posidonia Shale, the Amaltheen Shale and the Jurensis Marl are isotopically relatively heavy.

4.1.7 Mesozoic rocks in the Vienna Basin area

Rupprecht et al. (2017) studied Upper Jurassic Mikulov Marlstone from the very deep wells Maustrenk-ÜT1 and Zistersdorf-ÜT1. CSI patterns were determined by Rupprecht (2017). However, these patterns vary strongly, probably because of very high maturity (Table 5). Hence, it will be necessary to repeat these investigations in future.

4.2. Oil samples and oil-source correlations

4.2.1 Molasse Basin

Oil samples from 12 boreholes in the Voitsdorf Field, the largest oil field in the Molasse Basin (Boote et al., 2018), were studied in order to explore in-field variations. $\delta^{13}C$ ratios of n-alkanes and isoprenoids are listed in Table 6. These data show a very good fit (standard deviation: 0.1 to 0.3 ‰). This proves the reproducibility of the analytical results and shows that reservoir compartments are not present (or at least are not visible in oil composition).

Mean $\delta^{13}C$ ratios of 59 oil samples from the Upper Austrian part of the Molasse Basin are plotted in Fig. 7, where groups of oil are arranged from west (Mol-I) to east (Mol-VI). Voitsdorf oils are labelled as Mol-V. All oils show a distinct V-shape. This is clear evidence for their origin from the Schöneck Formation. Obviously the Eggerding Formation is not a major source rock for the Molasse oils, despite of its high source potential (see Sachsenhofer et al., 2010). In general, the oils become isotopically lighter from west to east (see also Gratzer et al., 2011 and Bechtel et al., 2013).

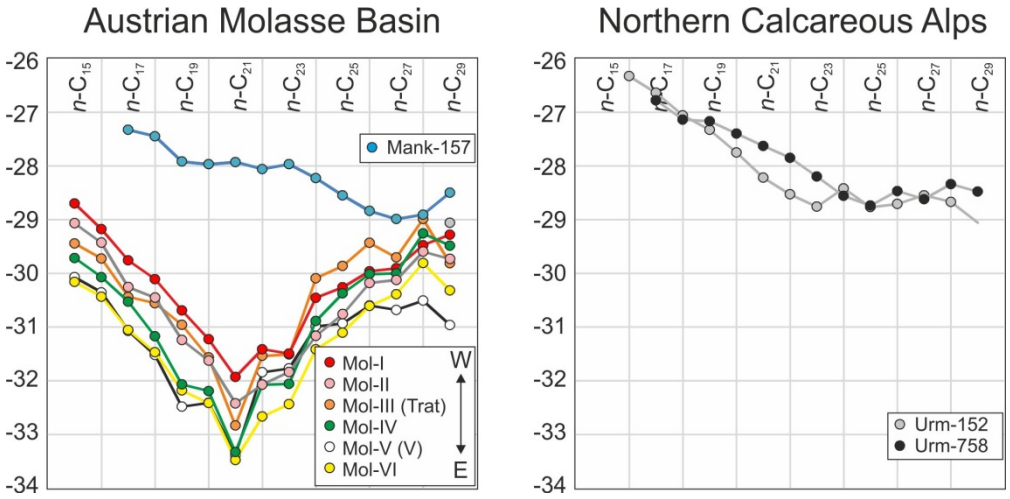

Fig. 7. Carbon isotopic composition ($\delta^{13}C$) of individual n-alkanes of oils from the Austrian Molasse Basin (Mol-I to Mol-VI are mean values of a total of 59 wells). Mank-1 represents oil stains in a well in Lower Austria. CSI patterns from oil stains in well Urmansau-1 (Northern Calcareous Alps) are shown for comparison.

In contrast, oil stains from the Molasse Basin in Lower Austria (Mank-1) show a different CSI pattern (Fig. 7). The lack of oleanane in this sample (see Appendix) suggests a pre-Cenozoic age of the source rock. Oleanane is also absent in oil recovered from 310 m depth in the Flysch Zone near Kleinraming-1 (Misch et al., 2017). This suggests that at least one additional source exists, probably within the Mesozoic succession of the Alpine nappe stack.

4.2.2 Northern Calcareous Alps

A significant oil seep in the Calcareous Alps at Urmannsau (Lower Austria) was used during Medieval times by monks from a nearby monastery as a fuel for lamps and for pharmaceutical purposes (Wessely, 2006). The oil seep led to the drilling of the exploration well Urmannsau 1, which penetrated Molasse units beneath the Alpine thrust front (Wessely, 2006). Although the well encountered oil and gas, commercial volumes of hydrocarbons were not discovered.

Oil stains at 152 and 758 m depth were studied within the frame of the present project. Oleanane could not be detected, but the oil stains yielded CSI patterns, which are very similar to that in the Mank 1 well (Fig. 7).

This finding supports the concept of Misch et al. (2017), which postulates a common source for the Urmannsau and Mank hydrocarbons (comp. Fig. 8).

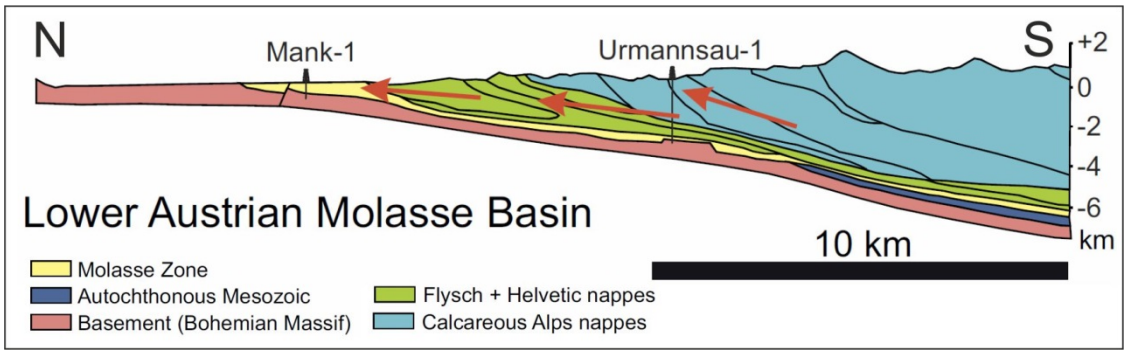

Fig. 8. Schematic north-south cross-sections through the Lower Austrian Molasse Basin (after Wessely, 2006). Arrows show possible migration pathways for liquid hydrocarbons which were detected in shallow wells and as surface seeps (Misch et al., 2017).

4.2.3 Autochthonous Mesozoic

Oil and oil stains from the Gresten Formation (Lower Qartzarenite Mbr.) in the Authochthonous Mesozoic were recovered from the Klement Field and the Kronberg well (see Fig. 1 for location).

Oil from the Klement Field is isotopically heavy, similar to oil from a Czech oil field in the Vienna Basin (Cz-1 in Fig. 9). Oil stains in cores from the Kronberg well show remarkably different CSI patterns (Fig. 9). The presence of two distinct oil phases is also supported by differences in n-alkane distributions and biomarker ratios.

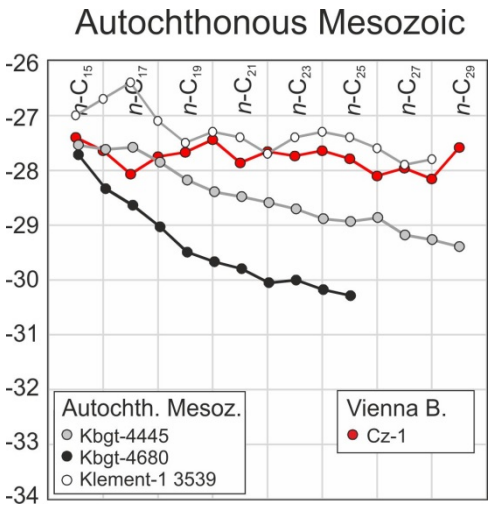

Fig. 9. Carbon isotopic composition ($\delta^{13}C$) of individual n-alkanes of oils from the Autochthonous Mesozoic (Klement-1, Kronberg-1). The CSI pattern of an oil from the Czech part of the Vienna Basin is shown for comparison.

5. CONCLUSIONS and OUTLOOK

CSI patterns of studied rock and oil samples units are summarized in Fig. 10. This figure shows that CSI patterns differ significantly depending on the stratigraphy of the investigated unit. CSI patterns of oil samples show similar high variations and – in case of the Molasse Basin – allow a clear oil-source correlation.

Nevertheless, the presented data can be only a starting point for future investigations. The following investigations seem especially promising:

- Investigation of additional organic matter-rich units:
    - Triassic "Seefeld Beds" (Northern Calcareous Alp; NCA)
    - Triassic Kössen Marl (NCA; rocks from a single outcrop in Tyrol turned out to be organic-lean. Hence it was not included in the frame of this project)
    - Cretaceous bituminous marls (Kainach Gosau)
    - Early Oligocene "bituminous marls" in the Inntal Valley (several samples have been investigated, but all analysed samples turned out to be very low in TOC).
- It has been proposed that Vienna Basin oils have been generated by Upper Jurassic (Mikulov Marlstone) and Oligocene rocks. Because of major differences, CSI patterns offer a powerful tool to distinguish different admixtures. Therefore, detailed investigations of the Mikulov Marlstone and oils in the Austrian (and Czech) part of the Vienna Basin seem useful.
- Oil at Mank, Urmannsau and Kleinraming(?) probably has the same Mesozoic source, which is neither the Reifling Limestone, nor the Bächental Bituminous Marl. We suggest a systematic investigation of the entire stratigraphy of the Northern Calcareous Alps to test its hydrocarbon potential.
- CSI patterns of Lower Oligocene rocks in the Molasse Basin show a clear stratigraphic trend. Despite of detailed investigations, the processes which result in different CSI patterns are still poorly understood and need additional investigations.

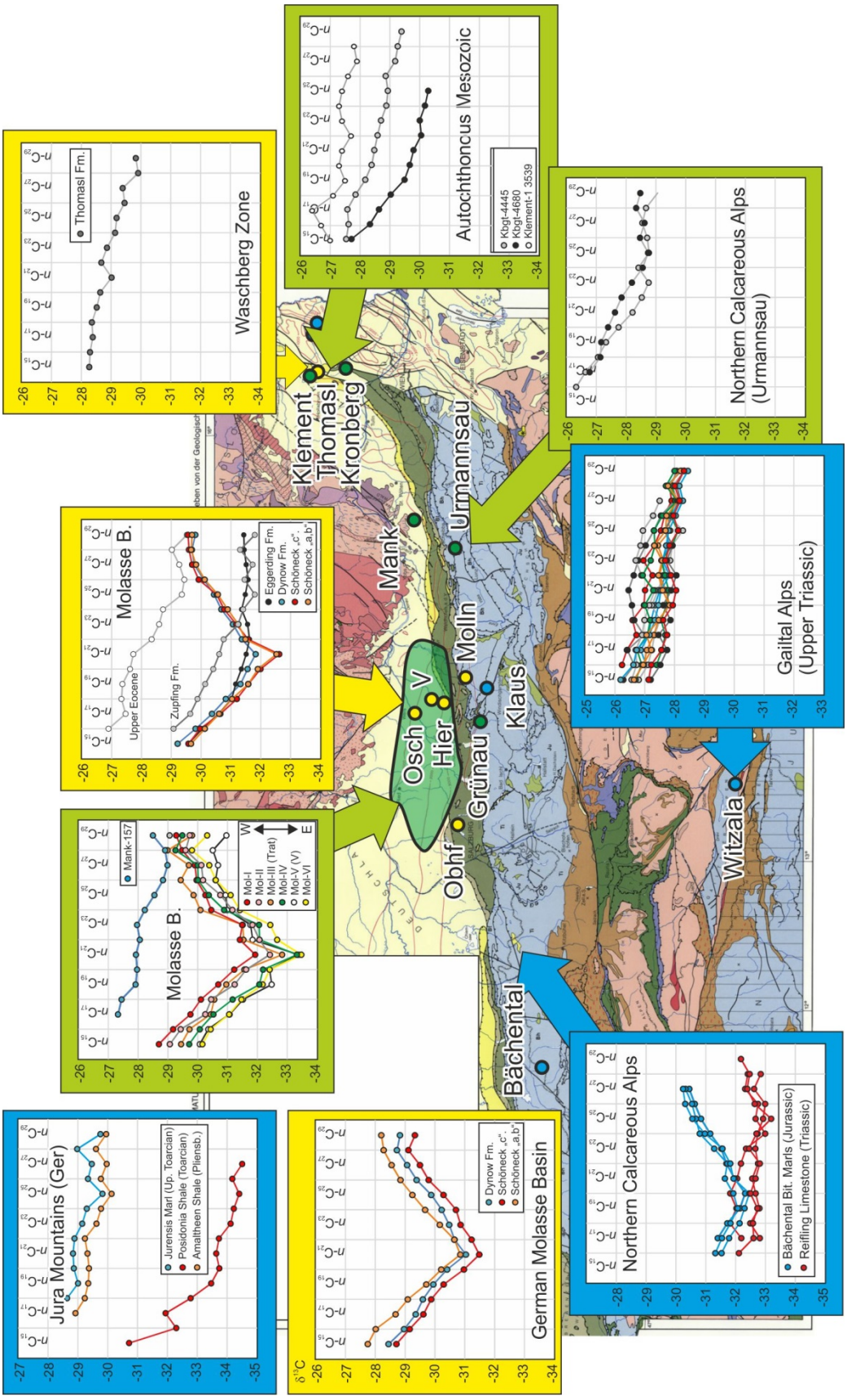

Fig. 10. Distribution of CSI patterns of Cenozoic (yellow background) and Mesozoic (blue) source rocks, as well as of oil samples and oil stains (green) (map: GBA).

6. REFERENCES

Abram, P., 2001. Sedimentologische und organisc-geochemische Aspekte des Oberen organisch reichen Hauptdolomites in den Gailtaler Alpen – Untersuchungen anhand eines Aufschlusses NE des Witzalas (Windische Höhe, Kärnten, Österreich). Unpubl. Master´s thesis, Montanuniversitaet Leoben, 103 pp.

Bechtel, A., Gratzer, R., Sachsenhofer, R.F., Gusterhuber, J., Lücke, A., Püttmann, W., 2008. Biomarker and carbon isotope variation in coal and fossil wood of Central Europe through the Cenozoic. Palaeogeography, Palaeoclimatology, Palaeoecology, 262, 166-175.

Bechtel, A.; Gratzer, R.; Linzer, H.-G., Sachsenhofer, R.F., 2013. Influence of migration distance, maturity and facies on the stable isotopic composition of alkanes and on carbazole distributions in oils and source rocks of the Alpine Foreland Basin of Austria. Org. Geochem., 62, 74-85.

Bechtel A., Gratzer R., Sachsenhofer R.F., 2017. Geochemical characteristics of oil samples provided by Geologisches Landesamt Bayern (Molasse Basin, Germany, Switzerland). Unpublished report.

Boote, D.R.D, Sachsenhofer, R.F., Tari, G., Arbouille, D., 2018. Petroleum Provinces of the Paratethyan Region. Journal Petroleum Geology, 41, 247-297.

Eglinton, G., Hamilton, R.J., 1967. Leaf epicuticular waxes. Science 156, 1322-1335.

Ficken, K.J., Li, B., Swain, D.L., Eglinton, G., 2000. An n-alkane proxy for the sedimentary input of submerged/floating freshwater aquatic macrophytes. Org. Geochem., 31, 745-749.

Fuchs, R., Hamrsmid, B., Kuffner, T., Peschel, R., Rögl, F., Sauer, R., Schreiber, O., 2001. Mid-Oligocene Thomasl Formation (Waschberg Unit, Lower Austria) – micropaleontology and stratigraphic correlation. – In: Piller, W.E., Rasser, M.W. (Eds.) Paleogene of the Eastern Alps. Verlag der Österreichischen Akademie der Wissenschaften, 14, 255-288, Wien.

Gratzer, R., Bechtel, A., Sachsenhofer, R.F., Linzer, H.-G., Reischenbacher, D., Schulz, H.-M., 2011. Oil–oil and oil–source rock correlations in the Alpine Foreland basin of Austria: insights from biomarker and stable carbon isotope studies. Marine and Petroleum Geology 28, 1171–1186.

Gratzer, R., Sachsenhofer, R.F., Bechtel, A, Gawlick, H.-J. (2015) Geogenic versus Anthropogenic: Hydrocarbons in the Spoil from the Falkenstein and Spering Tunnels (A9 Pyhrn Autobahn, Austria). Geomechanics and Tunnelling, 8, 356-363.

Grice, K., De Mesmay, R., Glucina, A., Wang, S., 2008. An improved and rapid 5A molecular sieve method for gas chromatography isotope ratio mass spectrometry of n-alkanes (C8–C30+). Org. Geochem., 39, 284–288

Hoefs, J., 2009. Stable Isotope Geochemistry. 6th Edition. Springer, Göttingen.

Lichtfouse E., Derenne S., Mariotti A., Largeau C., 1994. Possible algal origin of long chain odd n-alkanes in immature sediments as revealed by distributions and carbon isotope ratios. Org. Geochem., 22, 1023-1027.

Liu, H., Liu, W., 2016. n-Alkane distributions and concentrations in algae, submerged plants and terrestrial plants from the Qinghai-Tibetan Plateau. Org. Geochem., 99, 10-22.

Misch, D., Leu, W., Sachsenhofer, R.F., Gratzer, R., Rupprecht, B., Bechtel, A., 2017. Shallow hydrocarbon indications along the Alpine thrust belt and adjacent foreland basins: Distribution and implications for petroleum exploration. Journal Petroleum Geology, 40, 341-362.

Neumeister, S., Gratzer, R., Algeo, T.J., Bechtel, A., Gawlick, H.-J., Newton R., Sachsenhofer, R.F. (2015) Oceanic response to Pliensbachian and Toarcian magmatic events:

Implications from an organic-rich basinal succession in the NW Tethys. Global and Planetary Change, 126, 62-83.

Pedentchouk, N., Turich, C., 2017. Carbon and hydrogen isotopic compositions of *n*-alkanes as a tool in petroleum exploration. In: Lawson, M., Formolo, M. J. & Eiler, J. M. (eds) From Source to Seep: Geochemical Applications in Hydrocarbon Systems. Geological Society, London, Special Publications, 468, https://doi.org/10.1144/SP468.1

Pupp, M., 2018. Hydrocarbon potential of Eocene and Oligocene-Miocene source rocks of the Paratethys. PhD thesis Montanuniversitaet Leoben,152 pp.

Pupp, M., Bechtel, A., Gratzer, R., Heinrich, M., Kozak, S., Lipiarski, P., Sachsenhofer, R.F., 2018a. Depositional environment and petroleum potential of Oligocene rocks in the Waschberg Zone (Austria). Geologica Carpathica, 69, 410-436.

Radke, M. Willisch, H., Welte, D.H., 1980. Preparative hydrocarbon group type determination by automated medium liquid pressure chromatography. Anal. Chem., 52, 406-411.

Rupprecht, B., 2017. Hydrocarbon Generation and Alteration in the Vienna Basin. PhD thesis Montanuniversitaet Leoben, 169 pp.

Rupprecht, B.J., Sachsenhofer, R.F., Gawlick, H.-J., Kallanxhi, M.-E., Kucher, F., 2017. Jurassic source rocks in the Vienna Basin (Austria): Assessment of conventional and unconventional petroleum potential, Marine and Petroleum Geology, 86, 1327-1356.

Sachsenhofer, R.F., Leitner, B., Linzer, H.G., Bechtel, A., Coric, S., Gratzer, R., Reischenbacher, D., Soliman, A., 2010. Deposition, erosion and hydrocarbon source potential of the Oligocene Eggerding Formation (Molasse Basin, Austria). Austrian Journal of Earth Sciences, 103, 76-99.

Sachsenhofer R.F., Popov S.V., Coric, S., Mayer, J., Misch, D., Morton, M.T., Pupp, M., Rauball, J., Tari, G., 2018a. Paratethyan petroleum source rocks: An overview. Journal Petroleum Geology, 41, 219-245.

Sachsenhofer R.F., Popov S.V., Bechtel A., Coric S., Francu J., Gratzer R., Grunert P., Kotarba M., Mayer J., Pupp M, Rupprecht B.J., 2018b. Oligocene and Lower Miocene source rocks in the Paratethys: Palaeogeographic and stratigraphic controls. In: Simmons, M. (ed.) Petroleum Geology of the Black Sea. Geol. Soc. Spec. Publ., 464, 267–306.

Schulz, H.-M., Sachsenhofer, R.F., Bechtel, A., Polesny, H. and Wagner, L., 2002. The origin of hydrocarbon source rocks in the Austrian Molasse Basin (Eocene - Oligocene transition). Marine and Petroleum Geology, 19, 6, 683-709.

Sweda, M., 2018. Compound-specific carbon isotope analysis of n-alkanes from source rocks and oils from the Paratethyan realm. Unpubl. MSc thesis. Montanuniversitaet Leoben.

Wagner, L., 1980. Geologische Charakteristik der wichtigsten Erdöl- und Erdgasträger der oberösterreichischen Molasse, Teil I: Die Sandsteine des Obereozän. Erdoel-Erdgas-Zeitschrift, 96, 338-346.

Wagner, L.R., 1998. Tectono-stratigraphy and hydrocarbons in the Molasse Foredeep of Salzburg, Upper and Lower Austria. In: A. Mascle, C. Puifdefábregas, H.P. Luterbacher, and M. Fernández (eds.), Cenozoic Foreland Basins of Western Europe. Geological Society Special Publications, 134, 339-369.

Wehner, H., Kuckelkorn, K., 1995. Zur Herkunft der Erdöle im nördlichen Alpen-/ Karpatenvorland. Erdöl-Erdgas-Kohle, 111, 508-514.

Wessely, G., 2006. Niederösterreich. Geologie der österreichischen Bundesländer. Geologische Bundesanstalt, Vienna, 416 pp.

Appendix

Bulk organic geochemical parameters, concentration and concentration ratios of specific biomarkers of Oligocene source rocks from the Molasse Basin.

Sample	Formation	TOC (wt%)	HI	Tmax (°C)	Sat.HC (%)	Aro.HC (%)	N+A (%)	*n*-alk	*n*-C_{15-19}/ Σ*n*-alk.	*n*-C_{21-25}/ Σ*n*-alk.	*n*-C_{27-31}/ Σ*n*-alk.	CPI
W. Bavaria												
A-21	Dynow	2.37	644	432	27	19	54	5001	0.20	0.32	0.25	0.9
A-32	Schöneck c	8.58	637	436	35	17	49	5953	0.28	0.32	0.16	0.8
A-40	Schöneck c	4.30	514	430	41	13	46	9103	0.29	0.39	0.15	1.2
A-47	Schöneck c	2.15	473	428	37	17	46	5179	0.43	0.29	0.14	1.1
E. Bavaria												
C-01	Schöneck b	7.45	522	419	24	7	69	3560	0.26	0.34	0.23	1.6
C-09	Schöneck b	3.23	443	415	16	13	71	1180	0.46	0.19	0.23	1.6
C-14	Schöneck b	3.37	515	413	14	9	77	5905	0.48	0.21	0.21	1.6
Oberschauersberg												
1369.17	Eggerding	5.99	578	421	21	9	71	n.a.	0.37	0.26	0.24	1.0
1371.22	Eggerding	3.56	552	424	22	11	67	n.a.	0.35	0.27	0.29	1.5
1375.82	Dynow	2,39	600	425	17	14	69	1735	0.36	0.24	0.31	1.3
1377.28	Dynow	4,67	542	418	22	14	64	1625	0.32	0.24	0.34	1.3
1381.79	Schöneck c	2,39	600	425	21	15	63	1870	0.38	0.29	0.23	1.1
1385.45	Schöneck c	4.60	n.a.	n.a.	17	9	74	4896	0.37	0.34	0.19	1.5
1389.24	Schöneck b	2,95	501	411	12	10	78	596	0.30	0.27	0.32	1.9
1392.87	Schöneck a	2.00	399	417	11	14	74	977	0.32	0.25	0.33	1.6

								αααR+S Steranes		
Sample	Pr/Ph [rel.prop]	Pri/*n*-C17 [rel.prop]	Ph/*n*-C18 [rel.prop]	Steranes (µg/gTOC)	Hopanes (µg/gTOC)	St/ Hop	OI (%)	C_{27}/ ΣC_{27-29}St.	C_{28}/ ΣC_{27-29}St.	C_{29}/ ΣC_{27-29}St.
W. Bavaria										
A-21	2.21	4.98	2.25	1469	587	2.50	12.6	0.30	0.37	0.33
A-32	1.40	2.58	1.85	1428	2567	0.55	7.0	0.29	0.34	0.37
A-40	2.08	1.91	0.84	554	893	0.62	18.3	0.37	0.30	0.32
A-47	1.33	2.68	1.95	492	250	1.96	33.0	0.43	0.30	0.27
E. Bavaria										
C-01	0.71	1.24	1.28	1333	1126	1.16	16.0	0.35	0.31	0.33
C-09	0.91	3.75	4.14	1038	328	3.16	32.2	0.40	0.33	0.27
C-14	1.09	2.18	2.49	321	149	2.14	26.6	0.37	0.33	0.30
Oberschauersberg										
1369.17	0.67	4.35	5.41	n.a.	n.a.	7.92	24.4	0.24	0.43	0.34
1371.22	1.19	2.62	2.39	n.a.	n.a.	7.10	23.2	0.26	0.44	0.31
1375.82	3.64	10.58	2.82	619	809	0.77	10.8	0.28	0.42	0.30
1377.28	2.48	11.01	3.33	797	865	0.92	13.2	0.25	0.41	0.34
1381.79	2.86	9.09	1.39	870	1033	0.84	20.8	0.31	0.33	0.36
1385.45	0.81	3.53	3.86	1966	865	2.27	17.0	0.46	0.32	0.22
1389.24	1.31	7.06	4.40	634	380	1.66	34.9	0.40	0.30	0.30
1392.87	2.45	6.73	2.09	71	206	0.34	50.4	0.39	0.28	0.33

(TOC: total organic carbon; HI: hydrogen index in mg HC/g TOC; Sat.HC: saturated hydrocarbon; Aro.HC: aromatic hydrocarbons; N+A: NSO compounds + asphaltenes; n-alk: n-alkane concentration in µg/g TOC; CPI: carbon preference index; Pr/Ph: pristane/phytane ratio; St/Hop: steranes / hopanes; OI: oleanane index)

Bulk organic geochemical parameters, concentration and concentration ratios of specific biomarkers of cuttings samples from the Thomasl Formation (Waschberg Zone).

Sample	Formation	TOC (wt%)	HI	Tmax (°C)	Sat.HC (%)	Aro.HC (%)	N+A (%)	*n*-alk	*n*-C_{15-19}/ Σ*n*-alk.	*n*-C_{21-25}/ Σ*n*-alk.	*n*-C_{27-31}/ Σ*n*-alk.	CPI
THO-1650	1.88	165	424	30	27	5	69	1192	0.90	0.02	0.03	2.73
THO-1720	2.66	223	418	24	16	6	78	542	0.67	0.07	0.17	1.68
THO-1760	3.33	116	426	17	28	8	63	900	0.87	0.04	0.06	2.06

						αααR+S Steranes		
Sample	Pr/Ph [rel.prop]	Pri/*n*-C_{17} [rel.prop]	Ph/*n*-C_{18} [rel.prop]	Steranes (µg/g TOC)	Hopanes (µg/g TOC)	C_{27}/ ΣC_{27-29}St.	C_{28}/ ΣC_{27-29}St.	C_{29}/ ΣC_{27-29}St.
THO-1650	1.84	0.56	0.56	5	n.a.	0.39	0.22	0.40
THO-1720	1.63	0.81	0.87	60	n.a.	0.34	0.35	0.32
THO-1760	1.80	0.91	0.93	15	n.a.	0.34	0.30	0.36

(TOC: total organic carbon; HI: hydrogen index in mg HC/g TOC; EOM: extractable organic matter in mg/g TOC; Sat.HC: saturated hydrocarbons; Aro.HC: aromatic hydrocarbons; N+A: NSO compounds + asphaltenes; n-alk: n-alkane concentration in µg/g TOC; CPI: carbon preference index; Pr/Ph: pristane/phytane ratio; n.a.: no data)

Organic geochemical parameters, concentration ratios of specific biomarkers of Reifling Limestone (Falkenstein tunnel, Northern Calcareous Alps).

Sample	*n*-C_{15-19}/ Σ*n*-alk.	*n*-C_{21-25}/ Σ*n*-alk.	*n*-C_{27-31}/ Σ*n*-alk.	CPI	Pr/Ph [rel.prop]	Pri/*n*-C_{17} [rel.prop]	Ph/*n*-C_{18} [rel.prop]	OI (%)
Falkenstein tunnel								
KB-04	0.44	0.28	0.13	1.03	1.56	1.02	0.72	0
KB-05	0.43	0.28	0.14	0.89	1.61	1.01	0.69	0
KB-07	0.44	0.32	0.12	0.57	1.35	1.37	0.54	0

(CPI: carbon preference index, Pr/Ph: pristane/phytane ratio; OI: oleanane index)

Bulk organic geochemical parameters, concentration and concentration ratios of samples of the Bächental bituminous marls (Northern Calcareous Alps).

Sample	Gr (API°)	Sat.HC (%)	Aro HC (%)	N+A (%)	*n*-C_{15-19}/ Σ*n*-alk.	*n*-C_{21-25}/ Σ*n*-alk.	*n*-C_{27-31}/ Σ*n*-alk.	CPI	Pr/Ph	Pr/*n*-C17	Ph/*n*-C18	MPI-1	OI (%)
BT-35	9.40	666	0.26		0.30	0.32	1.24	0.91	3.58	4.20	1.0		0.80
BT-26	7.60	653	0.25		0.26	0.39	2.81	0.86	3.83	4.28	1.6		0.71
BT-25	12.90	622	0.20		0.28	0.39	2.09	0.86	3.53	3.97	1.1		0.77

	ααα R+S Steranes		
	C27/ ΣC27-29St.	C28/ ΣC27-29St.	C29/ ΣC27-29St.
BT-35	0.24	0.33	0.42
BT-26	0.26	0.31	0.43
BT-25	0.21	0.34	0.45

(TOC: total organic carbon; HI: hydrogen index in mg HC/g TOC; CPI: carbon preference index; Pr/Ph: pristane/phytane ratio; GI: gammacerane index; OI: oleanane index)

Organic geochemical parameters, concentration and concentration ratios of specific biomarkers of oils from the Molasse Basin.

Sample	Gr. (API°)	Sat.HC (%)	Aro HC (%)	N+A (%)	*n*-C_{15-19}/ Σ*n*-alk.	*n*-C_{21-25}/ Σ*n*-alk.	*n*-C_{27-31}/ Σ*n*-alk.	CPI	Pr/Ph	Pr/*n*-C17	Ph/*n*-C18	MPI-1[A]	OI (%)
Voitsdorf													
V-01	35	52	18	30	0.33	0.35	0.16	1.1	1.43	1.11	0.84	0.77	9.4
V-02	35	41	15	44	0.33	0.32	0.16	1.1	1.48	1.09	0.89	0.76	10.7
V-08	35	44	15	41	0.33	0.34	0.15	1.1	1.84	1.17	0.74	0.80	9.1
V-11	35	16	6	79	0.33	0.11	0.10	0.3	1.35	1.37	0.87	0.77	10.3
V-13	35	50	16	35	0.33	0.34	0.15	1.0	1.88	1.23	0.74	0.78	11.8
V-15	35	48	16	36	0.33	0.24	0.15	1.0	1.47	1.15	0.81	0.77	10.0
V-19	35	37	13	50	0.33	0.33	0.16	1.1	1.51	1.08	0.89	0.77	8.7
V-21	35	12	4	83	0.33	0.05	0.13	0.5	1.44	1.10	0.74	n.a	9.4
V-23	35	38	13	49	0.33	0.37	0.10	1.4	1.56	1.14	0.79	0.78	8.9
V-33	35	n.a.	n.a.	n.a	0.33	0.16	0.16	n.a.	1.50	1.12	0.77	0.79	10.5
V-39	35	49	18	34	0.33	0.34	0.14	1.0	1.85	1.15	0.72	0.78	11.0
V-41	35	48	17	35	0.33	0.24	0.13	1.4	1.88	1.26	0.72	0.78	10.1
Haidenbach													
HNB-1	n.a.	45	10	45	0.33	0.37	0.14	1.4	1.70	0.87	0.48		6.5
Mank													
Mank-157	n.a.	17	7	76	0.73	0.15	0.00	3.4	0.95	0.54	0.54	n.a.	0

(Gr: gravity; API: american petroleum institute; Sat.HC: saturated hydrocarbon; Aro.HC: aromatic hydrocarbons; N+A: NSO compounds + asphaltenes; CPI: carbon preference index; Pr/Ph: pristane/phytane ratio, MPI-1: methylphenanthrene index; OI: oleanane index)

Organic geochemical parameters, concentration ratios of specific biomarkers of oil stains from Urmannsau-1 (Northern Calcareous Alps).

Sample	*n*-C_{15-19}/ Σ*n*-alk.	*n*-C_{21-25}/ Σ*n*-alk.	*n*-C_{27-31}/ Σ*n*-alk.	CPI	Pr/Ph [rel.prop]	Pri/*n*-C_{17} [rel.prop]	Ph/*n*-C_{18} [rel.prop]	OI (%)
Urmannsau-1								
Urman-152	0.48	0.39	0.00	24.1	0.98	0.55	0.51	0
Urman-758	0.46	0.39	0.00	8.10	0.71	0.53	0.54	0

(CPI: carbon preference index, Pr/Ph: pristane/phytane ratio; OI: oleanane index)